frontiers | Frontiers in Energy Research

ORIGINAL RESEARCH
published: 11 August 2022
doi: 10.3389/fenrg.2022.964042

Extracting Unknown Parameters of Proton Exchange Membrane Fuel Cells Using Quantum Encoded Pathfinder Algorithm

Ning Li[1,2], *Guo Zhou*[3]*, *Yongquan Zhou*[1,2,4]*, *Wu Deng*[5] *and Qifang Luo*[1,2]

[1]College of Artificial Intelligence, Guangxi University for Nationalities, Nanning, China, [2]Guangxi Key Laboratories of Hybrid Computation and IC Design Analysis, Nanning, China, [3]Department of Science and Technology Teaching, China University of Political Science and Law, Beijing, China, [4]Xiangsihu College of Guangxi University for Nationalities, Nanning, China, [5]College of Electronic Information and Automation, Civil Aviation University of China, Tianjin, China

Proton exchange membrane fuel cell (PEMFC) is one of the most widely used fuel cell types. Accurate modeling of PEMFC can better facilitate the research of PEMFC and guide designers to design FC products that meet people's needs. The modeling problem of PEMFC can be transformed into a parametric optimization problem. In order to improve the exploration capability of the pathfinder algorithm, the concept of quantum computing is introduced and a new quantum coded pathfinder optimization algorithm (QPFA) is proposed. QPFA was applied to the extraction of parameters of NedStackPS6, BCS500W and 250W FC, and these models of PEMFC have been applied for commercial use. The experimental results were compared with seven recently proposed metaheuristics and recently published literature, showing the accuracy and high precision of QPFA in extracting PEMFC parameters.

Keywords: fuel cell model, extraction parameters, quantum coding, pathfinder algorithm, metaheuristic

OPEN ACCESS

Edited by:
Rongfang Wang,
Qingdao University of Science and Technology, China

Reviewed by:
Denghe Gao,
Qingdao University of Science and Technology, China
Xiao Xv,
Qingdao University of Science and Technology, China

***Correspondence:**
Guo Zhou
guo.zhou@live.com
Yongquan Zhou
yongquanzhou@126.com

Specialty section:
This article was submitted to Fuel Cells, Electrolyzers and Membrane Reactors, a section of the journal Frontiers in Energy Research

Received: *08 June 2022*
Accepted: *24 June 2022*
Published: *11 August 2022*

Citation:
Li N, Zhou G, Zhou Y, Deng W and Luo Q (2022) Extracting Unknown Parameters of Proton Exchange Membrane Fuel Cells Using Quantum Encoded Pathfinder Algorithm. Front. Energy Res. 10:964042. doi: 10.3389/fenrg.2022.964042

1 INTRODUCTION

Due to the air pollution and environmental changes caused by burning fossil fuels, green renewable energy is increasingly considered as an alternative energy source (Priya et al., 2018). The fuel cell is a new energy supply technology (Rezk et al., 2022). Several popular fuel cell products in the market can be divided into several types according to the type of electrolyte: proton exchange membrane FC (PEMFC) (Pourrahmani et al., 2019), alkaline FC (AFC) (Saebea et al., 2019), solid oxide FC (SOFC) (Chuahy and Kokjohn, 2019), phosphoric acid fuel cell (PAFC) (Guo et al., 2021), (Inci and Türksoy, 2019), and microbial fuel cell (MFC) (Sayed et al., 2021), (Ido and Kawase, 2020). PEMFC is the most widely used (Miao et al., 2020). A large number of PEMFCs use in transportation applications (Shaheen et al., 2021). These fuel cells have been used for a variety of purposes in power supply, the mathematical model of PEMFC accurately established to better promote the research of FC.

There are three main types of mathematical modeling for PEMFCs, theoretical (Ashraf et al., 2022), empirical (Busquet et al., 2004), and semi-empirical models (Amphlett et al., 1995). Accurate design and modeling of PEMFCs can help researchers design products that meet performance requirements and reduce production costs. Early researchers mainly used adaptive filters and black-box testing techniques to determine the parameters of PEMFC models. However, these methods have significant drawbacks, including poor accuracy and lack of flexibility. PFMFC has multi-variable and multi-peak nonlinear characteristics, and the operation of the PEMFC is accompanied by complex

behavior of gas, liquid and heat conduction (Yang et al., 2020), which will lead to complex and labor time costly application of conventional technology (Abdel-Basset et al., 2021a). Therefore, a new technique is urgently needed to solve the PEMFC parameter extraction problem. With the development in the field of artificial intelligence, metaheuristic algorithms have achieved good results in nonlinear system optimization problems, and the problem of extracting PEMFC parameters can be seen as an optimization problem to be solved (Kandidayeni et al., 2019).

Many researchers have investigated the PEMFC parameter extraction problem using metaheuristic algorithms. GA was first used to extract the parameters of PEMFC (Priya et al., 2015), (Zhang and Wang, 2018), However, GA has the disadvantages of slow convergence speed and high parameter sensitivity, so a new optimization algorithm particle swarm optimization algorithm is applied to the PEMFC parameter extraction (Salim et al., 2015). Gong and Cai (2013) employed a named ranking-based differential evolution to find the parameters of the PEMFC model. El-Fergany (2018a) used Slap Algorithms to extract parameters of two PEMFC models that have been applied to commercial reality. Rao et al. (2019) modeled PEMFC using shark odor optimization and proved the reliability of shark odor optimization using statistical methods. Chen and Wang (2019) proposed a cuckoo search algorithm (CS-EO) with an explosion operator and applied it to the PEMFC parameter extraction problem with success on four models of fuel cell cases. Priya and Rajasekar (2019) used the flower pollination algorithm for PEMFC model parameter extraction. Selem et al. (2020) applied MRFO to the problem of accurate extraction of uncertain parameters of PEMFC models. Rizk-Allah and El-Fergany (2021) proposed an improved and developed AEO (IAEO) applying it to PEMFC modeling and optimization. Gouda et al. (2021a) used the jellyfish search algorithm to extract the exact parameters of the PEMFC and experimented on three test cases with success. Gouda et al. (2021b) investigated the dynamic performance of the fuel cell using the basic pathfinder algorithm. Several other optimization algorithms have been successfully applied to the PEMFC parameter extraction problem, such as ICHOA (Abdel-Basset et al., 2021a), MVO (Fathy and Rezk, 2018), IFSO (Qin et al., 2020), PO (Diab et al., 2020), JAYA (Xu et al., 2019), SMO (Gupta et al., 2021), EO (Seleem et al., 2021), GBO (Elsayed et al., 2021), BMO (Abdel-Basset et al., 2021a), and so on. Although many metaheuristic algorithms have been applied to extract unknown parameters of PEMFC, according to the No free lunch theorem (Wolpert and Macready, 1997), no single algorithm can solve all engineering optimization problems. There is still room to improve the extraction accuracy of PEMFC parameters, so it is necessary for researchers to improve the meta-heuristic algorithm and apply it in the extraction of PEMFC parameters.

Pathfinder optimization algorithm is a metaheuristic algorithm proposed by Yapici and Cetinkaya (2019). It is inspired by the principle that the group leader leads other individuals to the optimal future regional in nature. Pathfinder optimization algorithm has been applied to many complex practical engineering optimization problems and achieved success. In this paper, in order to solve the problem that the individual follower will easily fall into a local optimum in pathfinder algorithm, a quantum coded pathfinder optimization algorithm is proposed to solve continuous optimization problems. In QPFA, the probability amplitude is used to represent the probability of qubits two states, and the probability amplitude is mapped to the optimization problem interval to calculate the fitness value of individuals. Each individual corresponds to two solutions of the optimization space, which expands the diversity of the population, effectively avoids the problem of easily falling into a local optimum in PFA, and increases the exploration ability of the algorithm. The updating strategies of the PFA and the quantum revolving gate are used to update the probability amplitude for algorithm iteration. Then QPFA is applied to extract unknown parameters of PEMFC. This paper's main contribution can be summarized as follows:

1) A novel quantum coding pathfinder optimization algorithm is proposed to extract unknown parameters of PEMFC.
2) Three real PEMFC cases, NedStackPS6, 500WFC and 250WFC, were solved successfully. The experimental results proving the superiority of QPFA in extracting unknown parameters of PEMFC.
3) The results extracted by QPFA were compared with the excellent metaheuristic algorithm. In order to improve the persuasion of this study, the parameter results extracted by QPFA were compared with the results of recently published literatures, and QPFA found the best results.

The structure of this article is as follows. **Section 2** describes the fuel cell model. **Section 3** explains the method of extracting unknown parameters of PEMFC by QPFA and an objective function of optimization. **Section 4** introduces the basic pathfinder algorithm (PFA). **Section 5** introduces the quantum coding pathfinder algorithm (QPFA). **Section 6** introduces the experimental results and analysis of QPFA applied to three real cases, and compares the results with some powerful optimization algorithms. **Section 7** is the summary of this paper and the prospect of the future work.

2 PROTON EXCHANGE MEMBRANE FUEL CELL MODEL

This section introduces the semi-empirical model of PEMFC proposed by Mann et al. (2000). Its validity has been verified in many previous studies**.** The voltage output of PEMFC can be calculated using **Eq. 1** (Mann et al., 2000).

$$V_{o-cell} = E_{nernst} - V_{act} - V_{\Omega} - V_{con} \tag{1}$$

where V_{o-cell} represents the output voltage of PEMFC, its unit of measure is V. E_{nernst} denotes the cell open circuit voltage in (V) that is derived from the Nernst equation. V_{act} means a potential for activation in (V). V_{Ω} is the ohm voltage drop in the circuit and V_{con} represents the concentration voltage loss in (V).

Assuming that all connected cells have the same polarization properties, when N_s multiple cells are connected in series to form the stack, the stacks output voltage stack in (V) is described by **Eq. 2**.

$$V_{o-stack} = N_s \cdot V_{o-cell} \tag{2}$$

Based on the Nernst equation and the magnitude of the change in temperature, E_{nernst} can be calculated by **Eq. 3**.

$$E_{nernst} = 1.22 - 8.5 \times \frac{\left(T - T'\right)}{10^4} + 4.3085 \times \frac{T\left[\ln\left(P_{H_2} \cdot P_{O_2}^{0.5}\right)\right]}{10^5} \tag{3}$$

where T is the operating temperature of the cell in Kelvins and $T \leq 100^{\circ}$C, $T' = 273.15$K. P_{H_2} and P_{O_2} are the hydrogen and oxygen partial regulating pressures in PFMFC, they use atm as the unit of measurement. Dynamic changes of external load will lead to changes in P_{H_2} and P_{O_2}, and their numerical changes can be calculated by **Eqs 4–6** respectively. When the fuel cell chooses natural air as oxidant for electrochemical reaction, P_{O_2} will be calculated by **Eq. 6**.

$$P_{H_2} = 0.5 \times F_{H_a} \times P_{H_2O} \times \left[\frac{P_a}{F_{H_a} \times P_{H_2O} \times \exp\left(\frac{4.192 I_c}{AT^{0.832}}\right)}\right] \tag{4}$$

$$P_{O_2} = F_{H_a} \times P_{H_2O} \times \left[\frac{P_c}{F_{H_a} \times P_{H_2O} \times \exp\left(\frac{4.192 I_c}{AT^{0.832}}\right)}\right] \tag{5}$$

$$P_{O_2} = P_c - F_{H_a} \times P_{H_2O} - \frac{0.79}{0.21} \times P_{O_2} \times \exp\left(\frac{4.192 I_c}{AT^{0.832}}\right) \tag{6}$$

where F_{H_a} and F_{H_c} are the humidity of the steam at the anode and cathode of the fuel cell. P_a and P_c are the anode and cathode inlet pressures (atm). I_c and A are the cell current in (A) and the membrane effective area in (cm^2), respectively. Furthermore, P_{H_2O} is the water vapor saturation pressure (atm), which is calculated by **Eq. 7**, its value is only affected by temperature T.

$$\lg P_{H_2O} = 2.95 \times \frac{T - T'}{100} - 9.18 \times \frac{\left(T - T'\right)^2}{10^5} + 1.44 \times \frac{\left(T - T'\right)^3}{10^7} - 2.18 \tag{7}$$

The electrochemical reaction in fuel cells is slow at the initial stage, and activation loss V_{act} is used to describe the process, V_{act} can be calculated from **Eq. 8**.

$$V_{act} = -\left[\omega_1 + \omega_2 T + \omega_3 T \log_{10}\left(C_{O_2}\right) + \omega_4 T \log_{10}\left(I_c\right)\right] \tag{8}$$

where ω_1, ω_2, ω_3 and ω_4 are the semi-empirical coefficient in the model, their units of measurement are V, VK^{-1}, VK^{-1} and VK^{-1}. C_{O_2} represents the oxygen concentration at the cathode catalytic layer in (mol/cm^3), which is expressed by **Eq. 9**.

$$C_{O_2} = \frac{P_{O_2} \times \exp\left(\frac{498}{T}\right)}{5.08 \times 10^6} \tag{9}$$

In addition, the concentration of hydrogen at the anode catalytic layer C_{H_2} in (mol/cm3) is described by **Eq. 10**.

$$C_{H_2} = \frac{P_{H_2} \times \exp\left(\frac{-77}{T}\right)}{10.9 \times 10^5} \tag{10}$$

The ohm voltage loss in the circuit is calculated by **Eq. 11**, in the polarization curve, it shows a linear relationship.

$$V_\Omega = I_c \left(R_W + R_I\right) \tag{11}$$

where R_W in (Ω) represents the resistance shown by electrons as they pass through the connections to the external circuit, which can be calculated from **Eq. 12**. R_I in (Ω) indicates the resistance shown by protons passing through membrane active area A (cm^2).

$$R_W = \eta_F\left(\frac{D}{A}\right) \tag{12}$$

where the thickness of the membrane is represented by D in (cm). The membrane's specific resistivity is represented by η_F in (Ω.cm), η_F can be calculated by **Eq. 13**, λ in **Eq. 13** represents the amount of water in the membrane.

$$\eta_F = \frac{181.6 \times \exp^{-1}\left(\frac{4.18 \times (T-303)}{T}\right) \times \left[1 + 0.03\left(\frac{I_c}{A}\right) + 0.062\left(\frac{T}{303}\right)^2\left(\frac{I_c}{A}\right)^{2.5}\right]}{\left(\lambda - 0.634 - \frac{3I_c}{A}\right)} \tag{13}$$

Finally, the concentration over-potential V con or mass transport losses will affect the I–V curve when the FC is overloaded, and this phenomenon can be calculated and described by **Eq. 14**.

$$V_{con} = -\varepsilon \log_{10}\left(\frac{\sigma_{\max} - \sigma}{\sigma}\right) \tag{14}$$

where ε is a parametric coefficient in (V), $\sigma_{\max}$ and σ are represents the actual and maximum cell current density in ($A.cm^{-2}$).

3 PROPOSED IDENTIFICATION STRATEGY

This section introduces a general framework for extracting PEMFC parameters using metaheuristic algorithm. The QPFA proposed in this paper will be applied to extracting PEMFC parameters. According to the semi-empirical PFMFC model introduced in the previous section, seven parameters in the equation are unknown, and there is a strong coupling between these parameters. For such an optimization problem with nonlinear constraints, the metaheuristic optimization algorithm is used to determine the best parameters. The objective function is of great significance for model parameter identification. In this paper, the sum of the squared error (*SSE*) between the actual output voltage and the estimated output voltage is chosen as the objective function. The optimal model parameters are extracted by minimizing the objective function. Objective function (*SSE*) can be calculated by **Eq. 15**.

$$OF_{SSE} = \min\left\{\sum_{R=1}^{N_c}\left(V_{actual}\left(N_c\right) - V_{\text{simulation}}\left(N_c\right)\right)^2\right\} \tag{15}$$

TABLE 1 | Upper and lower bounds of parameters.

Parameter to optimize	ω_1	ω_2	ω_3	ω_4	λ	ε	R_I
Lower bound	−1.19969	1	3.6	−2.60	10	1	0.0136
Upper bound	−0.8532	5	9.8	−9.54	24	8	0.5

where V_{actual} and $V_{\text{simulation}}$ are the actual PFMFC data and simulation fuel cell voltage, N_c is the number of data items retrieved.

The optimization variables are the unknown PEMFC parameters, which can be described as:

$$x = [\omega_1, \omega_2, \omega_3, \omega_4, \lambda, \varepsilon, R_I]$$

Every variable has upper and lower bounds as follow:

$$\omega_i^{\min} \le \omega_i \ge \omega_i^{\max} \ (i = 1, 2, 3, 4)$$
$$\lambda^{\min} \le \lambda \ge \lambda^{\max}$$
$$\varepsilon^{\min} \le \varepsilon \ge \varepsilon^{\max}$$
$$R_I^{\min} \le R_I \ge R_I^{\max}$$

The specific values of upper and lower bounds of parameters are listed in **Table 1**. A general framework for PEMFC parameter extraction using metaheuristic optimization algorithm is shown in **Figure 1**.

4 BASIC PATHFINDER ALGORITHM

In the PFA algorithm, each individual in the population will be placed in D - dimensional space. The individual in the most promising area is called the pathfinder, and the rest of the population will follow the pathfinder to search. This search model can be mathematically described by **Eq. 16**

$$x_n^{i+1} = x_n^i + W_1 \cdot \left(x_{n-1}^i - x_n^i\right) + W_2 \cdot \left(x_p^i - x_n^i\right) + \varepsilon \quad n \in [2, 3, \ldots N] \tag{16}$$

where i represents the current iteration, x_n represents the position of the follower of the population. W_1, W_2 are two randomly generated vectors calculated from **Eqs 17**, **18**, r_1 and r_2 are a uniformly distributed random number generated randomly between (0, 1). W_1, W_2 can control the weight of the follower moving to the pathfinder and the neighboring individuals in the population. ε is the vibrancy vector, and its calculation can be obtained from **Eq. 19**, Δ_{ij} is the distance between the i-th and the j-th position in population.

$$W_1 = \alpha \cdot r_1 \tag{17}$$
$$W_2 = \beta \cdot r_2 \tag{18}$$
$$\varepsilon = \left(1 - \frac{i}{i_{\max}}\right) \cdot u_1 \cdot \Delta_{ij}, \Delta_{ij} = \|x_i - x_{i-1}\| \tag{19}$$

The pathfinder updating position is obtained from **Eq. 20**

$$x_p^{i+1} = x_p^i + 2r_3 \times \left(x_p^i - x_p^{i-1}\right) + \eta \tag{20}$$

where x_p^{i+1} represents the position of the i+1 generation pathfinder, x_p^i is the location of the i-th pathfinder. x_p^{i-1} is the location of the i-1 generation pathfinder, i represents the number of current iterations, r_3 represents a random number in a uniform distribution at [0,1]. η is obtained from **Eq. 21**.

$$\eta = u_2 \cdot e^{\frac{-2i}{i_{\max}}} \tag{21}$$

where $i_{\max}$ represents the maximum iteration number, u_2 is a random number evenly distributed within the range of [-1,1]. The pseudo-code of pathfinder algorithm is in Algorithm 1.

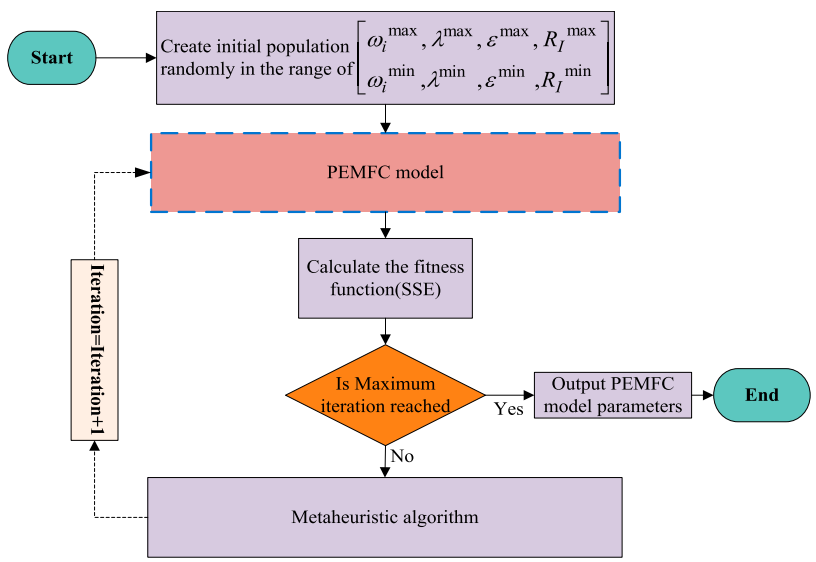

FIGURE 1 | Process of extracting PEMFC parameters with metaheuristic optimization algorithm.

Algorithm 1. Pseudo-code of the Pathfinder algorithm.

1. Initialize parameters of PFA, N_{pop}, i_{max}, dim
2. Set the population
3. Determine the fitness of initial population
4. Access the pathfinder's position
5. **While** i < MAX$_{iter}$
6. **Calculate** η, ε, W_1 and W_2
7. Update the coordinate of pathfinder using Eq.(20)
8. Check the line for pathfinder
9. **If** new pathfinder's score is better than the last
10. pathfinder = new pathfinder
11. **End** if
12. **For** n = 2 to N_{pop}
13. Update the position of follower using Eq.(16)
14. Check the line for follower
15. **If** new follower's score is better than the last
16. follower's position=new follower's position
17. **End** if
18. **End** for
19. Find new leader
20. $i = i+1$
21. **End** while
22. **End**

5 PROPOSED QUANTUM CODE PATHFINDER ALGORITHM

A quantum coding method is proposed by Li et al. (Shiyong, 2007), this paper adopts the quantum coding method proposed by Li et al. The probability amplitude of qubit is used to encode the position vector of individual population in QPFA, quantum revolving gate updates the quantum bit rotation angle. In order to avoid premature convergence of PFA, quantum not gate is added into the algorithm as mutation behavior.

5.1 Quantum Theory

Since the concept of quantum mechanical systems was introduced, researchers in many fields have devoted themselves to the study of quantum mechanics (Benioff, 1982). Quantum physics is the theoretical root of quantum computing, and Schrödinger's equation (SE) describes the intrinsic dynamics of quantum computing (Grover, 2001).

5.2 Qubit and Quantum Superposition

The smallest unit of information storage is called a qubit in quantum theory, qubits are the basic storage unit in quantum computing, and the Dirac symbol $|x\rangle$ is used to represent qubits. A qubit can have state $|0\rangle$ and state $|1\rangle$ or the linear combination of state $|0\rangle$ and state $|1\rangle$ (Shiyong, 2007), (Dey et al., 2014). The linear combination of state $|0\rangle$ and state $|1\rangle$ referred to as quantum superposition, this superposition is described by the wave function $|\Psi\rangle$ in Hilbert space. The wave function is described as:

$$|\Psi\rangle = \omega|0\rangle + \theta|1\rangle \tag{22}$$

where ω and θ are called the probability amplitude of the quantum state, ω and θ represents for when measuring a qubit, wave function $|\Psi\rangle$ collapse to $|0\rangle$ with a probability $|\omega|^2$, collapse to $|1\rangle$ with a probability $|\theta|^2$. ω and θ satisfy the constraint of **Eq. 23**.

$$|\omega|^2 + |\theta|^2 = 1 \tag{23}$$

According to **Eq. 23**, use the coding method of Li et al. (Shiyong, 2007), $\omega = \cos(\varphi), \theta = \sin(\varphi)$, φ is the rotation angle of a qubit.

5.3 Initial Population

When the population is initialized, the probability amplitude of qubit is directly used as the position vector of the individual in PFA algorithm, the individual population can be initialized as:

$$\left[P_m = \begin{bmatrix} \cos(\varphi_{m,1}) & \cos(\varphi_{m,2}) & \cdots & \cos(\varphi_{m,n}) \\ \sin(\varphi_{m,1}) & \cos(\varphi_{m,2}) & \cdots & \sin(\varphi_{m,n}) \end{bmatrix}\right] \tag{24}$$

where n = 1,2,. . .,D represents the dimensions of the problem, m = 1,2, . . . , N represents the population number of individuals in PFA, $\varphi_{m,n}$ is the rotation angle of qubits, $\varphi_{m,n}$ is initialed by **Eq. 25**.

$$\varphi_{m,n} = 2\pi \cdot rand(0,1) \tag{25}$$

Each individual in the QPFA corresponds to two positions in the problem space, they are calculated from the probability amplitude of qubits respectively, P_{iC} is calculated by the probability amplitude of quantum bit $|0\rangle$, P_{iS} is calculated by the probability amplitude of quantum bit $|1\rangle$.

$$\begin{aligned} P_{mC} &= \left(\cos(\varphi_{m,1}), \cos(\varphi_{m,2}), \ldots, \cos(\varphi_{m,j})\right) \\ P_{mS} &= \left(\sin(\varphi_{m,1}), \sin(\varphi_{m,2}), \ldots, \sin(\varphi_{m,j})\right) \end{aligned} \tag{26}$$

5.4 Solution Space Mapping

In QPFA, the search traversal space of the population individual is [−1,1] in every dimension. Since the form of qubit is used to represent the individual population in PFA, it is necessary to map the qubit to the optimization problem interval, the quantum bit's probability $|0\rangle$ and $|1\rangle$ correspond to the two solutions of optimization problem. The mapping process is accomplished through **Eqs 27**, **28**.

$$Y^n_{mC} = \frac{1}{2}\left[Y^n_{\max}\left(1 + \omega^n_N\right) + Y^n_{\min}\left(1 - \theta^n_m\right)\right] \tag{27}$$

$$Y^n_{mS} = \frac{1}{2}\left[Y^n_{\max}\left(1 + \omega^n_m\right) + Y^n_{\min}\left(1 - \theta^n_m\right)\right] \tag{28}$$

where Y^n_{mC} and Y^n_{mS} are calculated from the probabilities of qubits $|0\rangle$ and $|1\rangle$, respectively. Each qubit map to two positions in the solution space.

5.5 Individual Updates

In order to make use of the pathfinder search optimization algorithm to update rotation angle, the displacement difference of updating population individuals in the pathfinder search optimization algorithm is used to rewrite **Eqs 16**–**30**. In QPFA, the movement of individual population is carried out through the quantum revolving door, and the position update of individual population in PFA is transformed into the probability amplitude update of individual population qubit in QPFA.

5.5.1 Update of Qubit Angle on Individual

$$\Delta\varphi_{mn}^{p}(t+1) = \Delta\varphi_{mn}^{p}(t) + \Delta\varphi^{p} + \eta \tag{29}$$

$$\Delta\varphi_{mn}^{F}(t+1) = \Delta\varphi_{mn}^{F}(t) + W_1 \times \Delta\varphi^{F} + W_2 \times \Delta\varphi_{p}^{F} + \varepsilon \tag{30}$$

where t represents the current iteration, $\Delta\varphi^{p}$ represents the difference of the probability amplitude vector between the current pathfinder's position and the previous pathfinder's position. $\Delta\varphi^{F}$ represents the probability amplitude vector difference between the position of the current follower and the position of an adjacent follower. $\Delta\varphi_{p}^{F}$ represents the probability amplitude vector difference between the current follower position and the pathfinder position. $\Delta\varphi^{p}$, $\Delta\varphi_{ij}^{F}$ and $\Delta\varphi_{p}^{F}$ can be calculated as follows:

$$\Delta\varphi^{p} = \begin{cases} 2\pi + \varphi_p^n(t) - \varphi_p^n(t-1) & \varphi_p^n(t) - \varphi_p^n(t-1) < -\pi \\ \varphi_p^n(t) - \varphi_p^n(t-1) & -\pi \le \varphi_p^n(t) - \varphi_p^n(t-1) \le \pi \\ \varphi_p^n(t) - \varphi_p^n(t-1) - 2\pi & \varphi_p^n(t) - \varphi_p^n(t-1) > \pi \end{cases} \quad (n = 1, 2, \ldots, D) \tag{31}$$

$$\Delta\varphi^{F} = \begin{cases} 2\pi + \varphi_m^n - \varphi_{m-1}^n & \varphi_m^n - \varphi_{m-1}^n < -\pi \\ \varphi_m^n - \varphi_{m-1}^n & -\pi \le \varphi_m^n - \varphi_{m-1}^n \le \pi \\ \varphi_m^n - \varphi_{m-1}^n - 2\pi & \varphi_m^n - \varphi_{m-1}^n > \pi \end{cases} \quad m = 2, 3, \ldots, N.\ n = 1, 2, \ldots, D \tag{32}$$

$$\Delta\varphi_{p}^{F} = \begin{cases} 2\pi + \varphi_p^n - \varphi_m^n & \varphi_p^n - \varphi_m^n < -\pi \\ \varphi_p^n - \varphi_m^n & -\pi \le \varphi_p^n - \varphi_m^n \le \pi \\ \varphi_p^n - \varphi_m^n - 2\pi & \varphi_p^n - \varphi_m^n > \pi \end{cases} \quad (m = 2, 3, \ldots, N.\ n = 1, 2, \ldots, D) \tag{33}$$

where φ_p^n represents the angle of pathfinder individual in n-th dimension. φ_m^n represents the angle of the follower individual in n-th dimension.

5.5.2 Update of Qubit Probability Amplitude of Individual

In the quantum optimization algorithm, the quantum revolving gate is used to update the probability amplitude of the qubit. The quantum revolving gate is set as **Eq. 34**, and the updating of the probability amplitude of the qubit is realized by **Eq. 35**.

$$\kappa(\Delta\varphi) = \begin{bmatrix} \cos(\Delta\varphi) & -\sin(\Delta\varphi) \\ \sin(\Delta\varphi) & \cos(\Delta\varphi) \end{bmatrix} \tag{34}$$

$$\begin{bmatrix} \cos(\varphi(t+1)) \\ \sin(\varphi(t+1)) \end{bmatrix} = \kappa(\Delta\varphi(t+1)) \begin{bmatrix} \cos(\varphi(t)) \\ \sin(\varphi(t)) \end{bmatrix} \tag{35}$$

where $[\cos(\varphi(t)), \sin(\varphi(t))]^T$ and $[\cos(\varphi(t+1)), \sin(\varphi(t+1))]^T$ represents the probability amplitude before and after the update. $\varphi(t)$ and $\phi(t+1)$ represents the rotation angle before and after the update. Through the **Eq. 35**, $[\cos(\varphi(t+1)), \sin(\varphi(t+1))]^T$ can be calculated as **Eq. 36**. According to the trigonometric transformation formula **Eq. 36** can be rewritten as **Eq. 37**.

$$\begin{cases} \cos(\varphi(t+1)) = \cos(\Delta\varphi)\cos(\varphi(t)) - \sin(\Delta\varphi)\sin(\varphi(t)) \\ \sin(\varphi(t+1)) = \sin(\Delta\varphi)\cos(\varphi(t)) + \cos(\Delta\varphi)\sin(\varphi(t)) \end{cases} \tag{36}$$

$$\begin{cases} \cos(\varphi(t+1)) = \cos(\varphi + \Delta\varphi) \\ \sin(\varphi(t+1)) = \sin(\varphi + \Delta\varphi) \end{cases} \tag{37}$$

when the update is complete, two new locations for the individual will be created:

$$\begin{aligned} P_{mC} &= \left(\cos\left(\varphi_{m,1} + \Delta\varphi_{m,1}(t+1)\right), \ldots, \cos\left(\varphi_{m,n} + \Delta\varphi_{m,n}(t+1)\right)\right) \\ P_{mS} &= \left(\sin\left(\varphi_{m,1} + \Delta\varphi_{m,1}(t+1)\right), \ldots, \sin\left(\varphi_{m,n} + \Delta\varphi_{m,n}(t+1)\right)\right) \end{aligned} \tag{38}$$

5.6 Mutation of Behavior

In PFA algorithm, pathfinder has a great influence on the follower. In the middle and late stage of algorithm execution, the follower will closely follow the pathfinder to search, which will increase the probability of the algorithm falling into the local optimal solution. Although quantum coding improves the diversity of the population, it is still possible to fall into the local optimal solution. In order to better jump out when the population falls into the local optimal solution, a quantum not gate is added to mutate the population qubit. Mutation behavior is carried out through quantum not gates, quantum not gates are described by **Eq. 39**. The mutation operation is described by **Eq. 40**.

$$\begin{bmatrix} 0 & 1 \\ 1 & 0 \end{bmatrix} \begin{bmatrix} \omega \\ \theta \end{bmatrix} = \begin{bmatrix} \theta \\ \omega \end{bmatrix} \tag{39}$$

$$\begin{bmatrix} 0 & 1 \\ 1 & 0 \end{bmatrix} \begin{bmatrix} \cos(\varphi_{mn}) \\ \sin(\varphi_{mn}) \end{bmatrix} = \begin{bmatrix} \sin(\varphi_{mn}) \\ \cos(\varphi_{mn}) \end{bmatrix} \tag{40}$$

5.7 Quantum Coding Pathfinder Algorithm Pseudo Code

The pseudo-code of the Quantum Pathfinder algorithm as in Algorithm 2.

Algorithm 2. Pseudo-code of the Quantum Pathfinder algorithm.

Input parameter: N_{pop}, Max_iteration, Dim, Lb, Ub
Initial population use Eq.(24) and Eq.(25)
The probability amplitude of quantum bit is mapped to the optimization problem space using Eq.(26), Eq.(27) and Eq.(28).
Calculate the objective function value
Get the best solution's rotation angle ϕ_p^n
Pathfinder's position = $\left[\cos(\phi_p^n), \sin(\phi_p^n)\right]^T$.
While t < Max_iteration
  Calculate η, ε, W_1 and W_2
  Update pathfinder's rotation angle increment using Eq.(31)
  Update follower's rotation angle increment using Eq.(32) and Eq.(33)
  Update the probability amplitude of qubit through quantum rotation gate
  If rand < P_c
    Using quantum not gates for mutation
  End if
  Perform **Step 3** and **Step 4**
  Get the best solution's rotation angle ϕ_p^n
  New pathfinder's position = $\left[\cos(\phi_p^n), \sin(\phi_p^n)\right]^T$.
End while
Output the optimal solution
End

6 RESULTS AND DISCUSSION

In this section, QPFA is applied to extract unknown parameters of three types of fuel cells, which are respectively NedStackPS6, BCS 500 and 250W FC. The objective function is to minimize the sum of squares of the difference between real data and simulation data, which can be obtained by **Eq. 15**. The simulations were performed on the MATLAB 2016b platform and run on a CPU Core i5-7100 v5 (3.80 GHz) with 16 GB RAM. The specific process of extracting fuel cell location parameters using QPFA algorithm is shown in **Figure 2**. Three types of fuel cell parameters, specific operating environments, and data sets are obtained in the Ref (Li et al., 2020a), the upper and lower bounds of the extracted unknown parameters are listed in **Table 1**.

In order to better test the ability of QPFA to extract unknown parameters of fuel cells, it is compared with six other excellent meta-heuristic algorithms with the strong optimization ability, which are PFA (Yapici and Cetinkaya, 2019), JAYA (Rao, 2016), WOA (Mirjalili and Lewis, 2016), SCA (Mirjalili, 2016), PSO (Kennedy and Eberhart, 1995), GWO (Mirjalili et al., 2014), and SMA (Li et al., 2020b). Finally, the experimental results were compared with the recently published literature. Due to the execution characteristics of the metaheuristic algorithm, the results of each run are different. In order to better test the optimizing ability of the algorithm, the results of 30 runs are considered in the experimental verification. The population, number of all metaheuristic algorithms N_{pop} = 30 and the number of iterations $Maxiteration$ = 1000. The specific parameter values of each

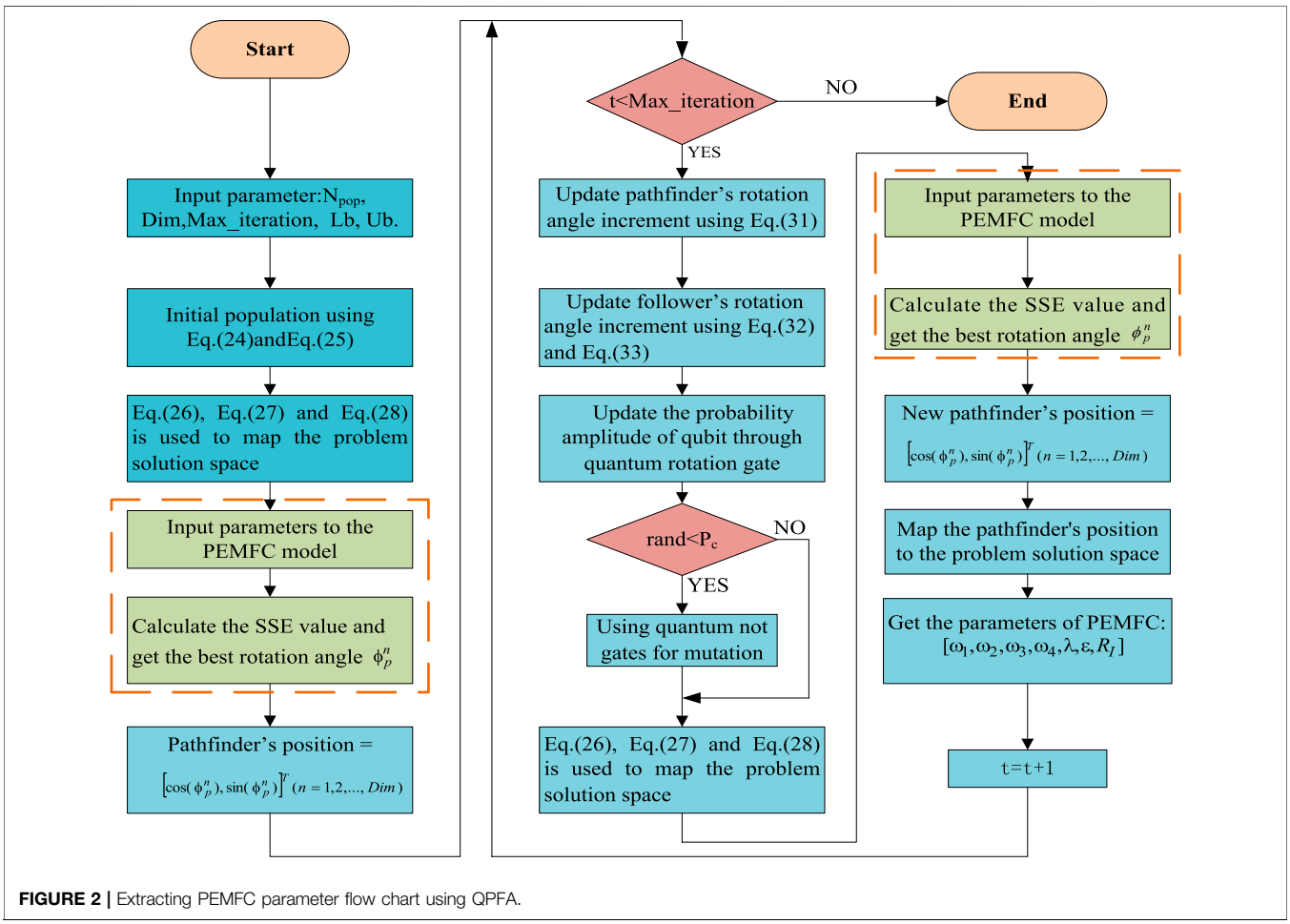

FIGURE 2 | Extracting PEMFC parameter flow chart using QPFA.

TABLE 2 | Specific parameters of the three PEMFCS.

PEMFC Name	N_{cell}	A (cm^2)	D (μm)	σ_{max} (A/cm^2)	T(K)	P_{H_2} (atm)	P_{O_2} (atm)
NedStackPS6	65	240	178	5	343	1	1
BCS 500W	32	64	178	0.469	333	1	0.2075
250W	24	27	178	0.860	343.15	1.0	1.0

TABLE 3 | SSE value obtained experimentally in Case1.

Algorithm	Parameter										
	ω_1 (V)	ω_2 (V/k)	ω_3 (V/k)	ω_4 (V/k)	λ	ε	R_l (mΩ)	SSE_{Best}	SSE_{Avg}	SSE_{Worst}	SSE_{Std}
PFA	−0.9082	4.53E-03	5.54E-05	−9.54E-05	12.6054	1.36E-02	1.05E-04	2.0797	2.08171	2.1131	0.04175
JAYA	−0.8532	4.22E-03	4.58E-05	−9.54E-05	12.7813	3.27E-02	1.00E-04	2.1803	2.2896	3.1655	0.29923
WOA	−1.1817	5.05E-03	3.76E-05	−9.54E-05	12.8164	2.68E-02	1.12E-04	2.1246	4.6200	5.9980	0.9438
SCA	−1.0667	4.99E-03	5.32E-05	−9.56E-05	13.1816	3.77E-02	1.32E-04	2.3398	3.9250	8.1258	1.2699
PSO	−0.9158	5.02E-03	9.27E-05	−9.54E-05	12.5836	1.71E-02	1.00E-04	2.4013	3.5004	13.5874	2.5540
GWO	−1.1446	5.01E-03	4.51E-05	−9.54E-05	12.7690	2.20E-02	1.12E-04	2.1152	2.6402	3.5747	0.4390
SMA	−0.8897	5.00E-03	9.79E-05	−9.54E-05	12.5745	1.36E-05	1.00E-04	2.0675	2.0952	2.3091	0.0625
QPFA	−0.9887	5.00E-03	7.65E-05	−9.54E-05	12.5743	1.36E-05	1.00E-04	**2.0656**	**2.0656**	**2.0656**	**5.55E-15**

**Bold numbers represent the best results.*

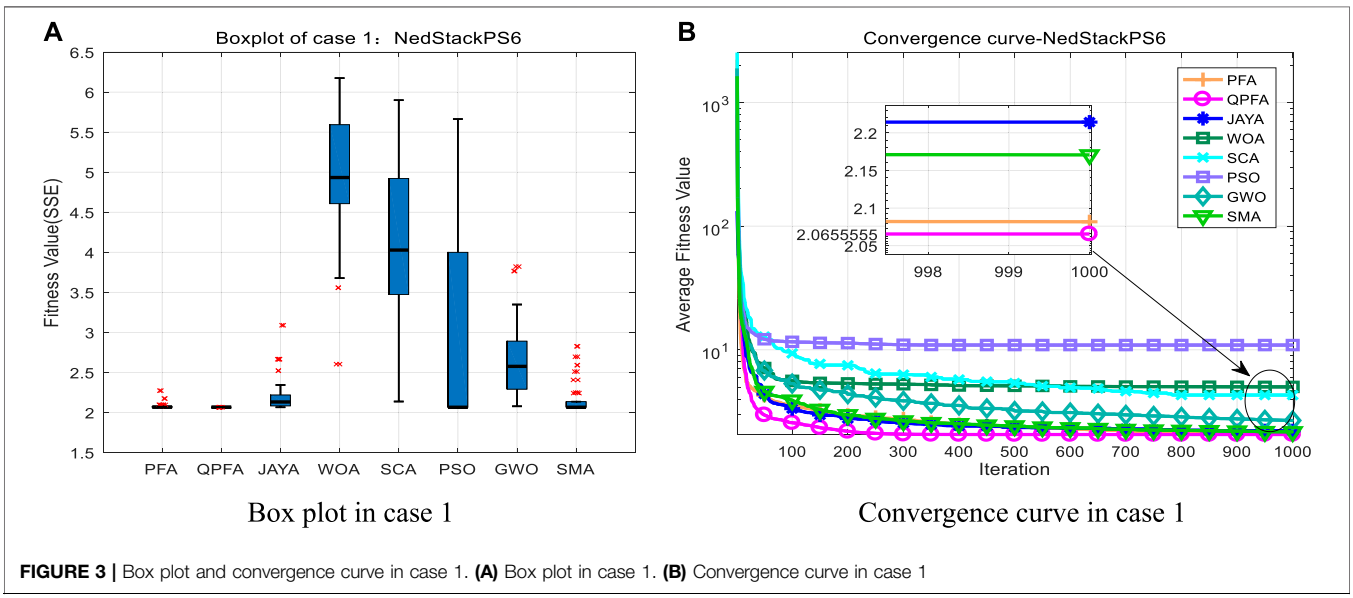

FIGURE 3 | Box plot and convergence curve in case 1. **(A)** Box plot in case 1. **(B)** Convergence curve in case 1

TABLE 4 | Comparison of real data and simulated data in Case 1.

N	Experimental data		Simulated data		*N*	Experimental data		Simulated data	
	I_{real} (A)	V_{real}(V)	$V_{simulated}$	$(V_{real}-V_{simulated})^2$		I_{real} (A)	V_{real}(V)	$V_{simulated}$	$(V_{real}-V_{simulated})^2$
1	2.250	61.640	62.35582	5.12394215E-01	16	110.300	47.520	47.63614	1.34888357E-02
2	6.750	59.570	59.78175	4.48398363E-02	17	117.000	47.100	47.04734	2.77273442E-03
3	9.000	58.940	59.05036	1.21785926E-02	18	126.000	46.480	46.25212	5.19287650E-02
4	15.750	57.540	57.49817	1.74951349E-03	19	135.000	45.660	45.44943	4.43414609E-02
5	20.250	56.800	56.71949	6.48106818E-03	20	141.800	44.850	44.83644	1.83896332E-04
6	24.750	56.130	56.04617	7.02683743E-03	21	150.800	44.240	44.01462	5.07967038E-02
7	31.500	55.230	55.15893	5.05161221E-03	22	162.000	42.250	42.97207	2.72552558E-01
8	36.000	54.660	54.62225	1.42531698E-03	23	171.000	41.660	42.11575	2.07707021E-01
9	45.000	53.610	53.6345	6.00487538E-04	24	182.300	40.680	41.01373	1.11373700E-01
10	51.750	52.860	52.94529	7.27426382E-03	25	189.000	40.090	40.34464	6.48427736E-02
11	67.500	51.910	51.44034	2.20578332E-01	26	195.800	38.510	39.65256	2.03221082E-02
12	72.000	51.220	51.027682	3.69862957E-02	27	204.800	38.730	38.71485	2.29421401E-04
13	90.000	49.660	49.41835	5.83931295E-02	28	211.500	38.150	37.99957	2.26289534E-02
14	99.000	49.000	48.62698	1.39146229E-01	29	220.500	37.380	37.01387	1.34050102E-01
15	105.800	48.150	48.03079	1.42121441E-02	SSE				2.0656

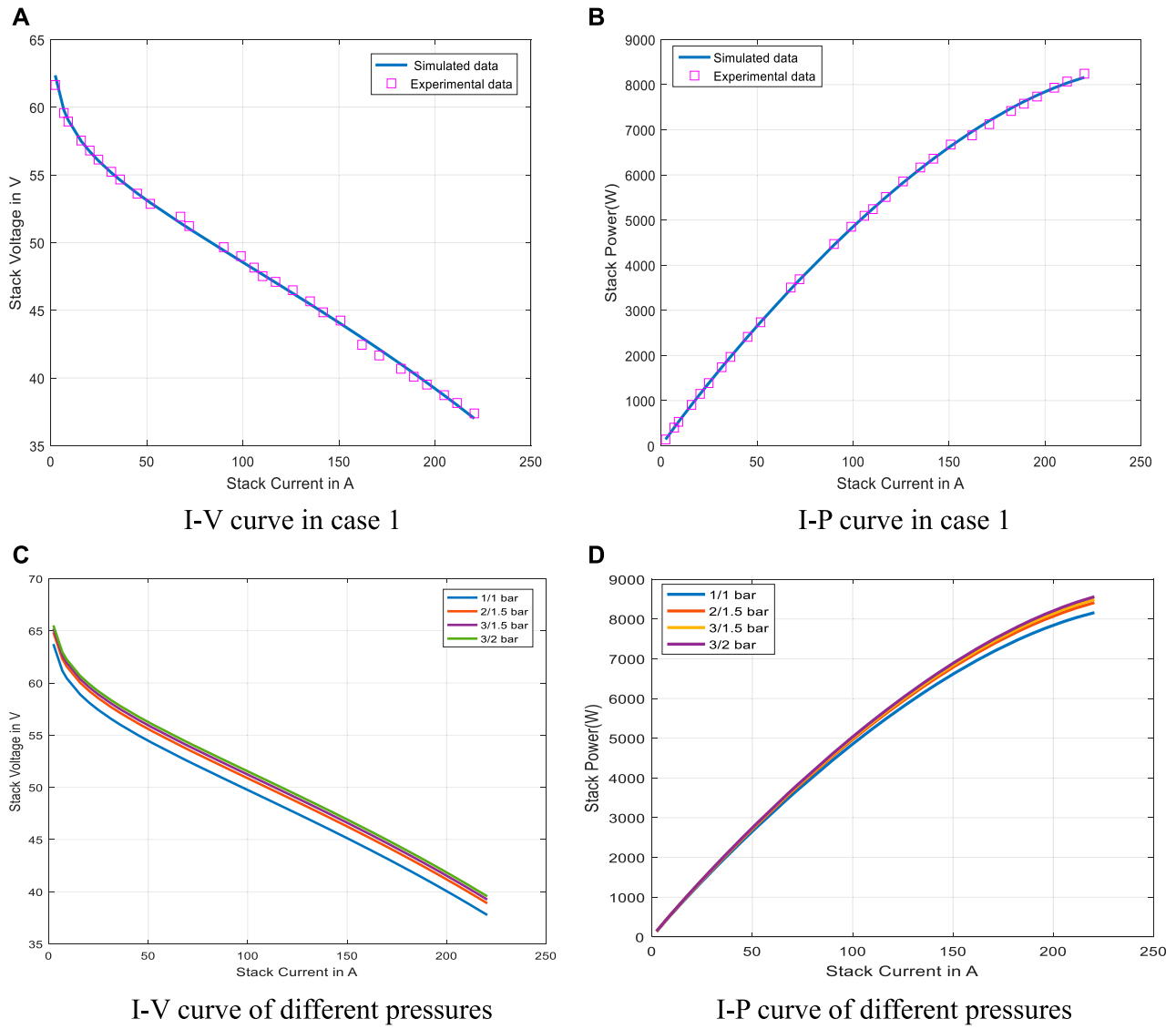

FIGURE 4 | Electrical characteristics of parameters extracted by QPFA on Case 1. **(A)** I-V curve in case 1 **(B)** I-P curve in case 1 **(C)** I-V curve of different pressures **(D)** I-P curve of different pressures.

metaheuristic algorithm are consistent with the settings of the original algorithm.

6.1 Case1: NedStackPS6

The technical parameters of NedStackPS6 are shown in the **Table 2**. According to the parameter extraction method as mentioned earlier, the parameter value of PEMFC obtained at the optimized minimum objective function will be the parameter to be extracted. Therefore, the performance of the optimization algorithm extracting PEMFC parameters can be judged by comparing the value of the objective function. After 30 runs, the experimental results obtained by QPFA and seven powerful optimization algorithms are shown in **Table 3**. **Table 3** lists the minimum objective function value (SSE_{Best}), average objective function value (SSE_{Avg}), worst objective function value (SSE_{Worst}), variance value (SSE_{Std}), and best PEMFC parameters value obtained by the optimization algorithm used in the experiment after 30 runs. As can be seen from **Table 3**, QPFA has achieved the best average value, the best value and the worst value. QPFA ranks the first among the eight algorithms. The box plot of the 30 running results is shown in **Figure 3A**, which shows that QPFA has good stability. In order to intuitively see the convergence speed performance of the algorithm, the average convergence curve of 30 running results is drawn in **Figure 3B**. It can be seen that QPFA's convergence speed is very fast, and its convergence curve is always at the bottom of the convergence curve of other algorithms, and finally achieves the best average objective function value in 1000 generations.

Table 4 shows each real data point and the simulated data point values calculated by the parameters extracted from QPFA, and the square of the difference between them (SSE) is also

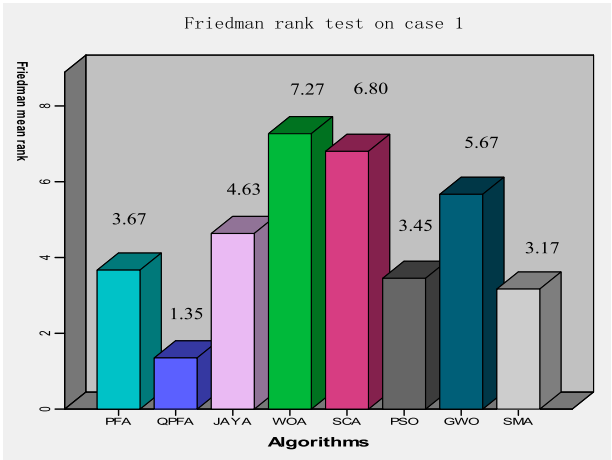

FIGURE 5 | Friedman test on Case 1.

listed. PEMFC's I-V curve and I-P curve obtained by QPFA is shown in the **Figures 4A,B** and . It can be seen from the simulated data curve and real discrete data points that the simulated data curve calculated by the parameter values given by QPFA fit the real discrete data points curve well. However, there are still some errors. In the activation and start-up stage of fuel cell, SSE reaches the maximum error: 5.12394215E-01, which may be because the output voltage PEMFC drops steeply and a lot of electrochemical reaction takes place in the initial stage. With the continuous output voltage of PEMFC, in the ohm region with linear voltage attenuation, their errors gradually decrease, and the minimum SSE value reaches 1.83896332E-04. In the third stage of PEMFC, concentration losses, SSE fluctuated with the increase of currency, but it was still within the acceptable range. In general, the NedstackPS6 parameter value extracted by QPFA well simulates the current-voltage polarization curve of NedstackPS6, and the error value is within an acceptable range. Based on the modeling PEMFC parameters extracted from QPFA, numerical simulation was carried out P_{H_2}/P_{O_2}= 1/1bar, 2/1.5 bar, 3/1.5 bar and 3/2 bar. The experimental results are consistent with the actual situation that the higher the pressure, the higher the output voltage of the battery stack. The I-V curve and I-P curve of the battery stack is shown in the **Figures 4C,D**. In order to better detect the optimization performance of QPFA, the Friedman test statistical analysis was conducted on the results of 30 times of optimization. As shown in the **Figure 5**, QPFA ranked first with the lowest rank value 1.35, proving that the optimum performance of QPFA ranked first. **Table 5** lists parameters extracted by QPFA and

TABLE 5 | Compare the QPFA on case 1 with the reference paper.

Algorithm	Parameter										
	ω_1 (V)	ω_2 (V/k)	ω_3 (V/k)	ω_4 (V/k)	λ	ε	R_l (mΩ)	SSE_{Best}	SSE_{Avg}	SSE_{Worst}	SSE_{Std}
SSO (El-Fergany, 2018a)	−0.9719	3.34E-03	7.91E-05	−9.54E-05	13.0000	5.34E-02	1.00E-04	2.18067	NA	2.25060	0.0203
MRFO (Selem et al., 2020)	−1.05602	3.13E-03	4.61E-05	−9.58E-05	20.18817	5.47E-02	1.66E-04	2.88702	6.82161	26.37778	4.90253
ABCDE (Hachana and El-Fergany, 2022)	−1.07813	3.38E-03	5.96E-05	−9.54E-05	13.09471	1.36E-02	1.00E-04	2.079165	2.079165	2.079165	6.6500E-15
TSO (Hachana and El-Fergany, 2022)	−0.8532	2.46E-03	3.94E-05	−9.54E-05	14.1357	1.13E-01	1.09E-04	2.219	NA	NA	NA
VSDE (Fathy et al., 2020a)	−1.1212	3.34E-03	4.67E-05	−9.54E-05	13.0000	4.94E-02	1.00E-04	2.08849	NA	NA	NA
MHHO (Yousri et al., 2021)	−1.1997	3.50E-03	3.67E-05	−9.54E-05	13.1930	1.36E-02	1.00E-04	2.0834	2.1614	2.5148	9.3800E-02
SFLA (Kandidayeni et al., 2019)	−1.02307	3.47E-03	7.75E-05	−9.54E-05	15.03229	1.36E-02	1.62E-04	2.167055	NA	NA	NA
GA (El-Fergany, 2018b)	−1.1997	3.41E-03	3.60E-05	−9.54E-05	13.0000	3.59E-02	1.37E-04	2.40896	NA	NA	NA
AEO (Rizk-Allah and El-Fergany, 2021)	−1.1993	4.27E-03	9.80E-05	−9.54E-05	15.0028	2.7E-02	1.17E-04	2.3069	3.0585	3.6245	0.4680
IAEO (Rizk-Allah and El-Fergany, 2021)	−0.9822	3.59E-03	9.48E-05	−9.54E-05	13.4650	1.36E-02	1.00E-04	2.1459	NA	NA	NA
BSOA (Cao et al., 2019)	−1.1997	4.24E-03	9.7999E-05	−9.54E-05	24.0000	1.71E-02	1.00E-04	6.4402	NA	NA	6.4402
JSA (Gouda et al., 2021a)	−1.1163	3.78E-03	8.03E-05	−9.54E-05	13.4650	1.36E-02	1.00E-04	2.1457	NA	NA	NA
IHBO (Abdel-Basset et al., 2021b)	−0.85396	2.40E-03	3.60E-05	−9.54E-05	13.465	1.36E-02	1.00E-04	2.14570	2.14570	2.14570	5.69E-10
QPFA	−0.9887	5.00E-03	7.65E-05	−9.54E-05	12.5743	1.36E-02	1.00E-04	2.0656	2.0656	2.0656	**5.55E-15**

**Bold numbers represent the best results.*

TABLE 6 | SSE value obtained experimentally on Case2.

Algorithm	Parameter										
	ω_1 (V)	ω_2 (V/k)	ω_3 (V/k)	ω_4 (V/k)	λ	ε	R_l (mΩ)	SSE_{Best}	SSE_{Avg}	SSE_{Worst}	SSE_{Std}
PFA	−0.9088	3.99E-03	4.44E-05	−1.92E-05	22.1675	1.62E-02	2.23E-04	0.0118056	0.0124511	0.0142374	7.56E-04
JAYA	−0.8532	4.66E-03	9.80E-05	−1.90E-04	23.1760	1.36E-02	4.63E-04	0.1366704	4.0890170	4.4372629	1.1210
WOA	−1.1257	5.01E-03	7.01E-05	−1.94E-04	24.0000	1.71E-02	2.06E-04	0.0134658	0.6715241	3.3504174	9.68E-01
SCA	−1.1070	4.99E-03	6.83E-05	−1.88E-04	22.0059	1.80E-02	2.07E-04	0.0416014	0.1651855	0.4893579	1.06E-01
PSO	−1.1845	4.60E-03	3.60E-05	−1.93E-04	20.8772	1.61E-02	1.00E-04	0.0116977	0.2126646	5.6549338	1.0279
GWO	−1.1768	4.90E-03	5.41E-05	−1.93E-04	21.5540	1.62E-02	1.40E-04	0.0117873	0.0151235	0.0251069	3.80E-03
SMA	−0.9819	5.01E-03	9.80E-05	−1.92E-04	21.7181	1.60E-02	1.97E-04	0.0118135	0.0137266	0.0199428	2.01E-03
QPFA	−1.1038	4.60E-03	5.06E-05	−1.93E-05	20.8772	1.61E-02	1.00E-04	**0.0116977**	**0.0116977**	**0.0116977**	**1.13E-16**

**Bold numbers represent the best results.*

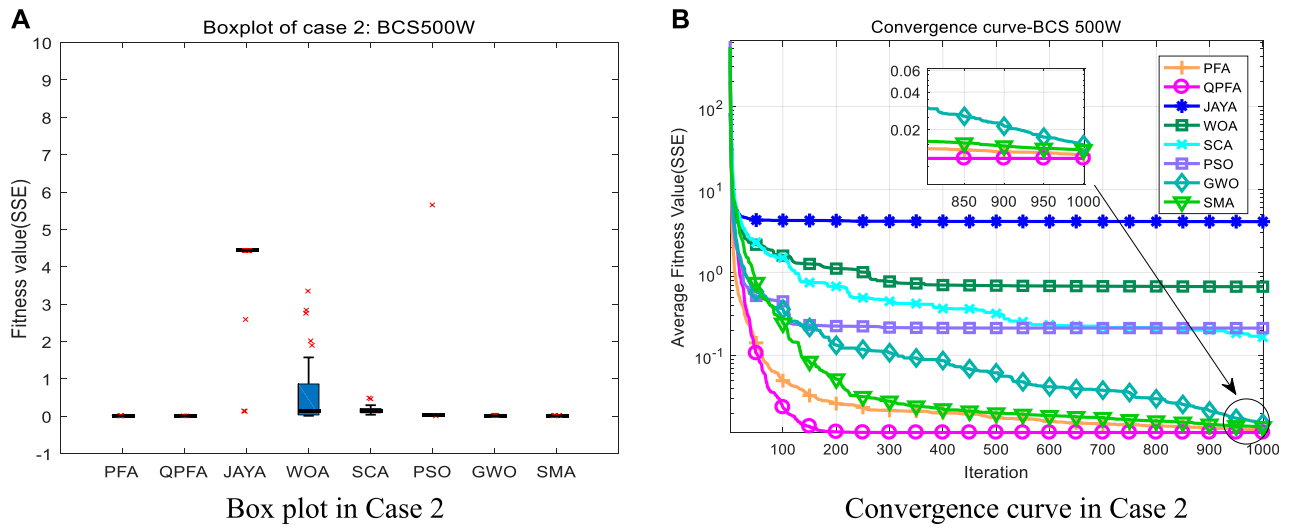

FIGURE 6 | Box plot and convergence curve in Case 2. **(A)** Box plot in Case 2 **(B)** Convergence curve in Case 2.

TABLE 7 | Comparison of real data and simulated data in Case 2.

N	Experimental data		Simulated data		*N*	Experimental data		Simulated data	
	I real (A)	Vreal(V)	Vsimulated	(Vreal-V simulated)2		I real (A)	Vreal(V)	Vsimulated	(Vreal-V simulated)2
1	0.600	29.000	28.99722	7.710066E-06	10	15.730	21.090	20.98774	1.045679E-02
2	2.100	26.310	26.30594	1.650749E-05	17	17.020	20.680	20.69451	2.105234E-04
3	3.580	25.090	25.09356	1.263969E-05	18	119.110	20.220	20.23099	1.206927E-04
4	5.080	24.250	24.25462	2.134710E-05	19	21.200	19.760	19.77094	1.197561E-04
5	7.170	23.370	23.37542	2.933361E-05	20	23.000	19.360	19.36602	3.629781E-05
6	9.550	22.570	22.58461	2.135978E-04	21	25.080	18.860	18.86647	4.181348E-05
7	11.350	22.060	22.07133	1.283099E-04	22	27.170	18.270	18.27472	2.228400E-05
8	12.540	21.750	21.75846	7.163051E-05	23	28.060	17.950	17.95331	1.096127E-05
9	13.730	21.450	21.46126	1.268454E-04	24	29.260	17.300	17.29288	5.073946E-05
					SSE				0.0116977

parameters in recent published literature, comparing the SSE values obtained after optimization with the published literature in recent years, QPFA get a better result than these powerful optimizers.

6.2 Case2: BCS 500W

A named BCS 500W fuel cell is used in this case to extract parameters, **Table 2** lists the specific parameters of this model. After 30 runs, the experimental results obtained by QPFA and

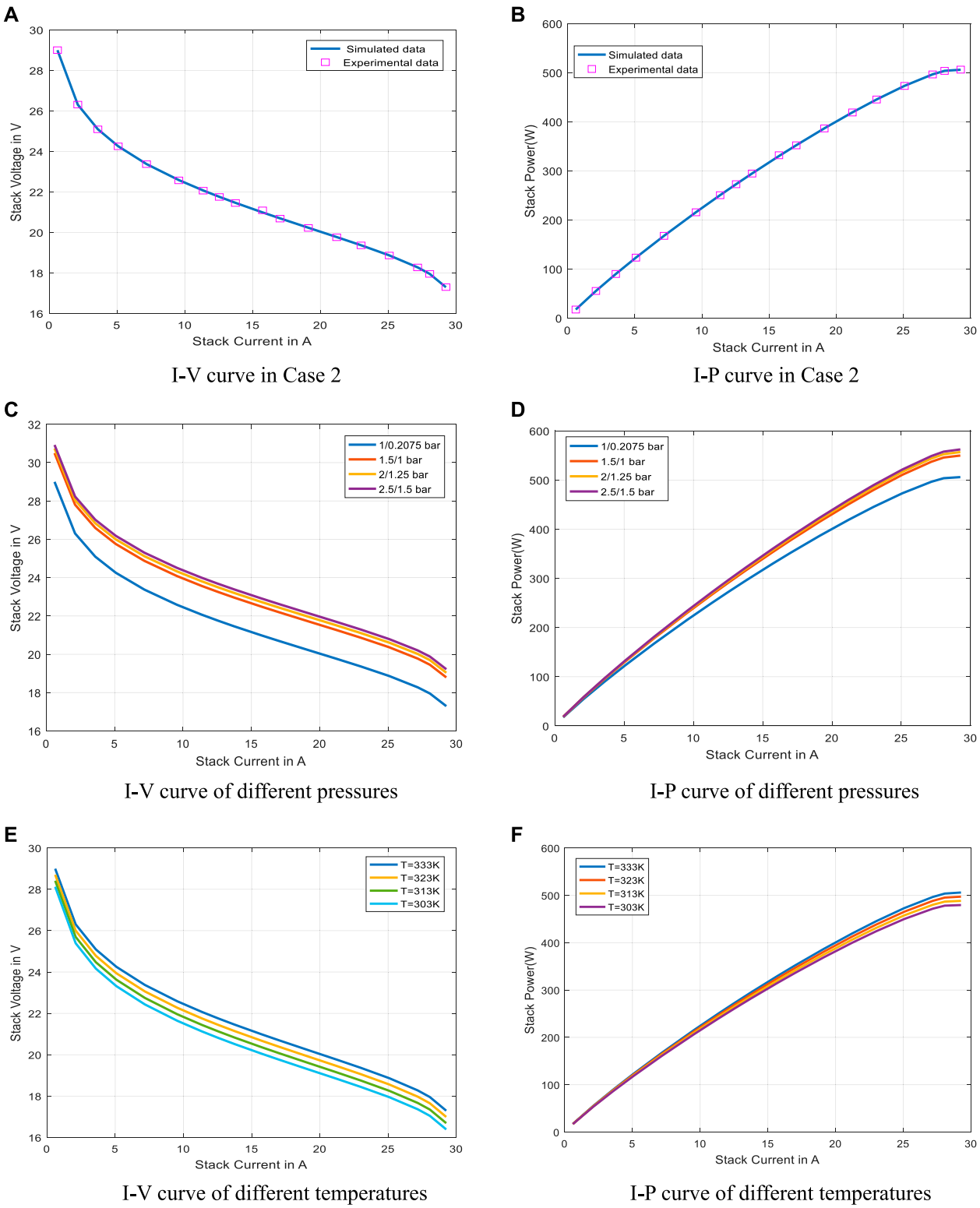

FIGURE 7 | Electrical characteristics of parameters extracted by QPFA on Case 2 **(A)**. I-V curve in Case 2 **(B)**. I-P curve in Case 2 **(C)**. I-V curve of different pressures **(D)**. I-P curve of different pressures **(E)**. I-V curve of different temperatures **(F)**. I-P curve of different temperatures.

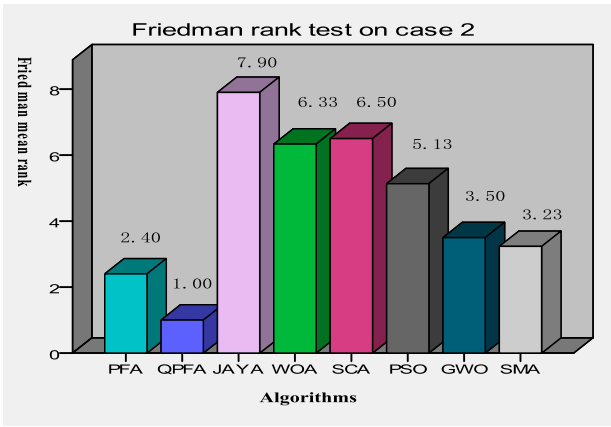

FIGURE 8 | Friedman test on case 2.

seven powerful optimization algorithms are shown in **Table 6**, this table shows the fitness values obtained by each algorithm and lists the parameter values corresponding to the best fitness values, QPFA has achieved the best average value, the best value and the worst value. The box plot of the 30 running results is shown in the **Figure 6A**, which shows that QPFA has better stability than other algorithms. The average convergence curve of 30 running results is drawn in **Figure 6B**. It can be seen that QPFA's convergence speed is very fast, and it converges to the minimum mean fitness at the end of the iteration.

Table 7 shows each real data point and the simulated data point values calculated by the parameters extracted from QPFA, and the square of the difference between them (SSE) is listed. PEMFC's polarization curve obtained by QPFA is shown in **Figure 7A**, PEMFC's I-P curve is also shown in **Figure 7B**. In order to better verify the correctness of PEMFC parameters extracted by QPFA, numerical simulation of the model was carried out under the condition of P_{H_2}/P_{O_2} = 1/0.2075bar, 1.5/1bar, 2/1.25bar and 2.5/1.5 bar. I-V and I-P curves under different conditions are shown in **Figures 7C,D**. The results show that increasing the pressure of hydrogen and oxygen increases the output voltage and power of the battery stack. BCS500W models at different temperatures were also studied, I-V and I-P curves are shown in **Figures 7E,F**. The results show

TABLE 8 | Compare the QPFA on case 2 with the reference paper.

Algorithm	Parameter										
	ω_1 (V)	ω_2 (V/k)	ω_3 (V/k)	ω_4 (V/k)	λ	ε	R_l (mΩ)	SSE_{Best}	SSE_{Avg}	SSE_{Worst}	SSE_{Std}
SSO (El-Fergany, 2018a)	−0.8532	4.81-03	9.43E-05	−1.92E-05	23.0000	1.58E-02	3.49E-04	0.01219	NA	0.01520	8.711E-04
WCMFO (Ben Messaoud, 2021)	−0.8532	1.62E-03	3.60E-07	−1.92E-05	4	1.64E-02	0.0017941	0.012233	NA	0.45416	0.081137
VSDE (Hasanien et al., 2022)	−1.1970	4.23E-03	9.79E-05	−1.92E-04	20.194	1.57E-02	1.10E-04	0.01214	NA	NA	NA
SFLA (Kandidayeni et al., 2019)	−0.9657	3.47E-03	7.78E-05	−9.54E-05	15.0322	1.36E-02	1.62E-04	0.011697	NA	0.011697	5.03E-08
FOA (Kandidayeni et al., 2019)	−1.0356	2.95E-03	3.76E-05	−9.54E-05	15.0296	1.36E-02	1.62E-04	0.011819	NA	0.030233	4.172E-03
HHO (Mossa et al., 2021)	−1.09311	3.28041E-03	5.67E-05	−1.89E-04	20.0436	151.48E-02	2.25E-04	0.014879	NA	NA	NA
SSO (Rao et al., 2019)	−1.018	2.3151E-03	5.24E-05	−1.2815E-04	18.8547	1.36E-02	7.5036E-04	7.1889	NA	NA	NA
MRFO (Selem et al., 2020)	−1.11262	3.06E-03	4.23E-05	−1.95E-04	21.705	1.718E-02	1.11E-04	0.03683	0.39107	1.13428	0.25386
IHBO (Selem et al., 2020)	−1.19970	3.31E-03	4.20E-05	−1.93E-04	20.877	1.613E-02	1.00E-04	0.01170	0.01174	0.01175	6.00E-05
MFO (Fathy et al., 2020b)	−1.0079	3.32E-03	7.98E-05	−1.90E-04	20.9189	1.58E-02	1.54E-04	0.0119	0.0478	0.1351	0.0455
JSA (Gouda et al., 2021a)	−0.96887	2.693E-03	4.67E-05	−1.90E-04	20.8389	1.6111E-02	1.00E-04	0.011699	0.011999	0.012279	0.000166
JADE (Diab et al., 2021)	−0.9035	3.4247E-03	5.2197E-05	−1.9173E-04	20.8167	1.61E-02	2.5759E-04	0.011556	NA	NA	NA
BSOA (Cao et al., 2019)	−0.9941398	2.6144E-03	3.6288E-05	−1.7200E-04	19.799895	1.36E-02	8.0E-04	4.4430	NA	NA	NA
QPFA	−1.1038	4.60E-03	5.06E-05	−1.93E-04	20.8772	1.61E-02	1.00E-04	**0.0116977**	0.0116977	**0.0116977**	**1.13E-16**

**Bold numbers represent the best results.*

TABLE 9 | *SSE* value obtained experimentally on case3.

Algorithm	Parameter										
	ω_1 (V)	ω_2 (V/k)	ω_3 (V/k)	ω_4 (V/k)	λ	ε	R_l (mΩ)	SSE_{Best}	SSE_{Avg}	SSE_{Worst}	SSE_{Std}
PFA	−0.9718	3.99E-03	3.60E-05	−1.21E-05	24.0000	6.31E-02	1.00E-04	0.6103529	0.6109617	0.6222137	2.15E-03
JAYA	−0.8532	443E-03	9.77E-05	−9.54E-05	17.9000	5.88E-02	8.00E-04	0.9151293	0.9170588	0.9276728	2.7E-03
WOA	−1.1564	5.10E-03	7.53E-05	−1.20E-04	23.3514	6.28E-02	1.01E-04	0.6125997	0.7837051	1.0527705	9.68E-01
SCA	−1.1997	5.00E-03	6.67E-05	−1.22E-04	21.5602	6.00E-02	1.00E-04	0.7149883	0.8436228	1.0587128	9.87E-02
PSO	−1.0475	5.01E-03	9.80E-05	−1.21E-04	24.0000	6.31E-02	1.00E-04	0.6103414	0.9875362	5.6348136	1.22E+00
GWO	−1.0235	4.63E-03	7.09E-05	−1.21E-04	23.9856	6.30E-02	1.01E-04	0.6105449	0.6184790	0.6345232	6.66E-03
SMA	−1.1969	5.00E-03	6.68E-05	−1.21E-04	24.0001	6.31E-02	1.00E-04	0.6103437	0.6115994	0.6160648	1.99E-03
QPFA	−0.9934	4.60E-03	8.81E-05	−1.30E-05	12.9868	6.17E-02	1.00E-04	**0.5934830**	**0.6102414**	**0.6103414**	**7.00E-04**

**Bold numbers represent the best results.*

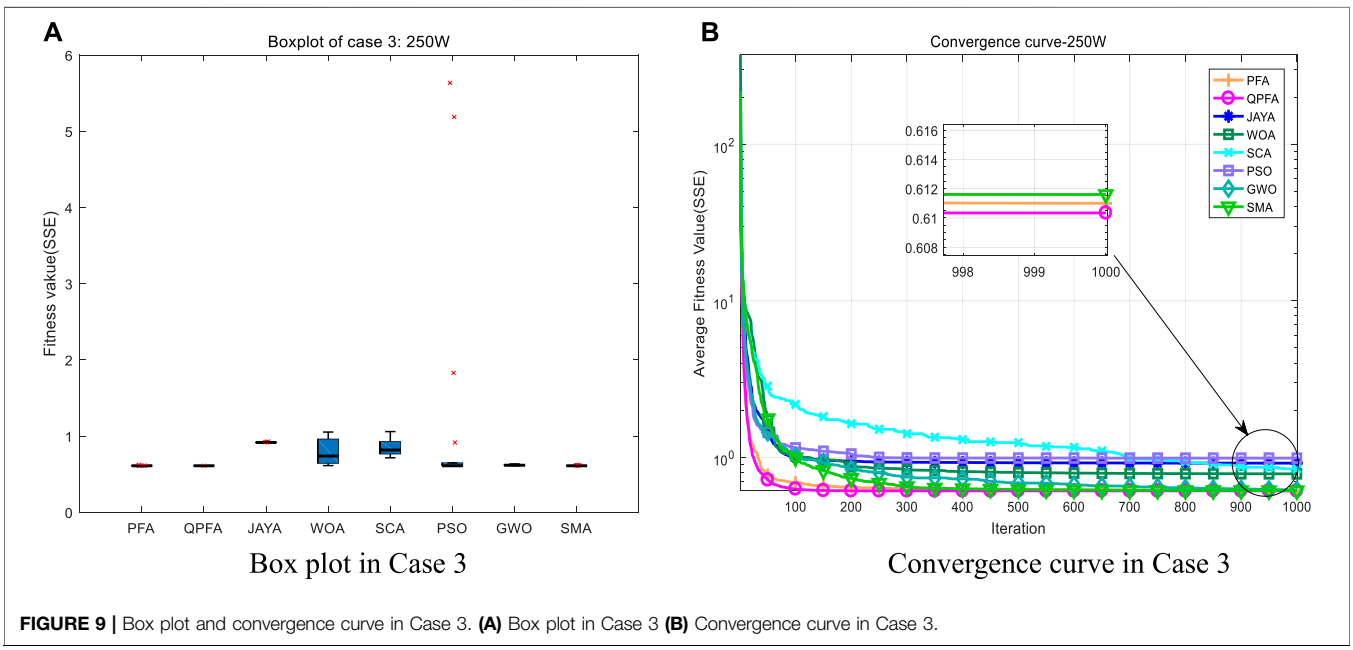

FIGURE 9 | Box plot and convergence curve in Case 3. **(A)** Box plot in Case 3 **(B)** Convergence curve in Case 3.

TABLE 10 | Comparison of real data and simulated data in Case 3.

N	Experimental data		Simulated data		N	Experimental data		Simulated data	
	I_{real} (A)	V_{real}(V)	$V_{simulated}$	$(V_{real}-V_{simulated})^2$		I_{real} (A)	V_{real}(V)	$V_{simulated}$	$(V_{real}-V_{simulated})^2$
1	0.2046	21.5139	21.598476	7.153164E-03	9	13.4720	15.1411	15.256408	1.329585E-02
2	1.2619	19.6737	19.544114	1.679258E-02	10	16.1494	14.4634	14.396836	4.430801E-03
3	2.6433	18.7154	18.612327	1.062401E-02	11	17.4795	14.087	13.896349	3.634792E-02
4	3.9734	17.9449	18.032021	7.590035E-03	12	18.8438	13.5792	13.294339	8.114588E-02
5	5.3206	17.5497	17.562585	1.660145E-04	13	20.1739	12.6772	12.557718	1.427605E-02
6	6.7019	17.1545	17.141268	1.750810E-04	14	21.5382	10.8743	11.466107	3.502361E-01
7	8.0491	16.6843	16.760232	5.765600E-03	15	22.9025	8.9213	8.776188	2.105739E-02
8	10.7265	15.8752	16.031494	2.442771E-02	SSE				0.5934830

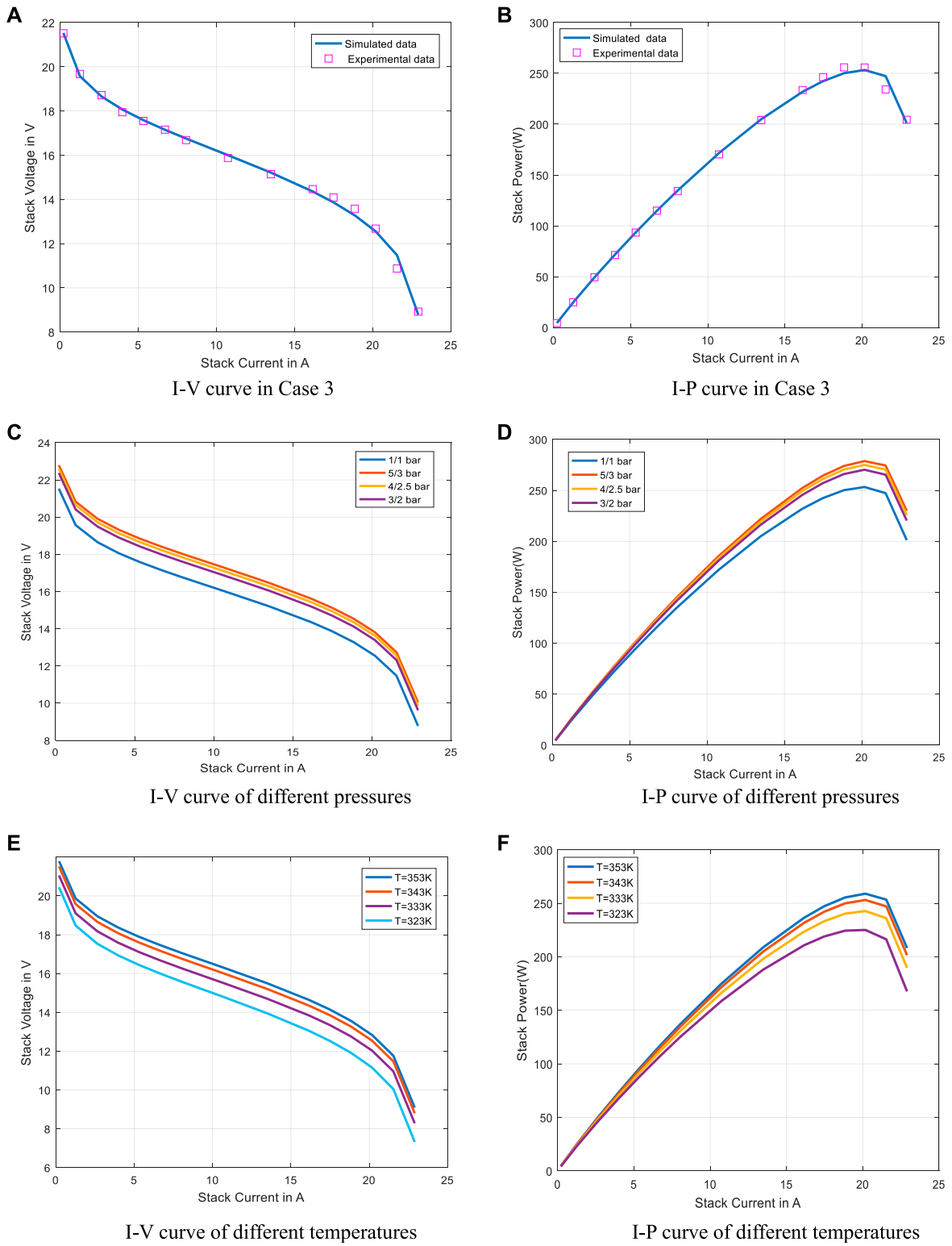

FIGURE 10 | Electrical characteristics of parameters extracted by QPFA on Case 3 **(A)**. I-V curve in Case 3 **(B)**. I-P curve in Case 3 **(C)**. I-V curve of different pressures **(D)**. I-P curve of different pressures **(E)**. I-V curve of different temperatures **(F)**. I-P curve of different temperatures.

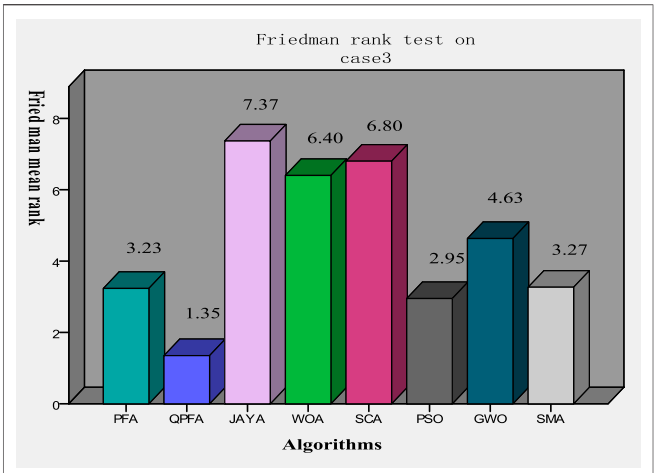

FIGURE 11 | Friedman test on case 3.

that improving the temperatures of battery stack can improve the output voltage and output power, which is consistent with the actual situation.

The Friedman test statistical analysis was conducted on the results of 30 times of optimization. As shown in **Figure 8**, QPFA ranked first with the lowest rank value 1.00, proving that the optimization performance of QPFA ranked first. **Table.8** lists parameters extracted by QPFA and parameters in recent published literature, comparing the SSE values obtained after optimization with the published literature in recent years, QPFA get a better result than these powerful optimizers.

6.3 Case3: 250W PEMFC

In order to better prove the excellent performance of QPFA in extracting PEMFC parameters, QPFA and other algorithms have been applied for extracting the model parameters of the 250W stack. The fitness function values after 30 runs are listed in **Table 9**, and the optimal parameter values found by each meta-heuristic algorithm are also given. After 30 times of running QPFA to extract the optimization problem of PEMFC parameters, QPFA obtained the minimum fitness function value, indicating that QPFA extracted the optimal PEMFC parameters. **Figure 9A** is the variance diagram of parameter extraction of 250W PEMFC. It can be seen that QPFA has very small variance and excellent stability. **Figure 9B** is the algorithms convergence diagram in the 250W PEMFC parameter extraction experiment. It can be seen that QPFA ranked first in the convergence speed at the beginning of iteration. As the algorithm continues to iterate, QPFA continues to search and optimize, and finally obtains the minimum average fitness function value at the end of iteration. **Table. 10** lists the real values of 250W and the values obtained by numerical simulation after parameters were extracted from QPFA to establish the model. SSE is also calculated point by point in **Table.10**. **Figures 10A,B** are I-V and I-P curves drawn by the parameters obtained by QPFA. Experimental results at different pressures and temperatures are shown in **Figures 10C–F**, the results show that increasing pressure and temperature can result in higher voltage and higher power output of the battery stack. The Friedman test statistical analysis was conducted on the results of 30 times of optimization. As shown in **Figure 11**, QPFA ranked first with the lowest rank value 1.35. **Table.11** lists parameters extracted by QPFA and parameters in recent published literature, comparing the SSE values obtained

TABLE 11 | Compare the QPFA on case 3 with the reference paper.

Algorithm	Parameter										
	ω_1 (V)	ω_2 (V/k)	ω_3 (V/k)	ω_4 (V/k)	λ	ε	R_l (mΩ)	SSE_{Best}	SSE_{Avg}	SSE_{Worst}	SSE_{Std}
HO (Fathy et al., 2021)	−0.48579	1.4215E-03	5.3464E-05	−1.397E-04	14.9236	2.085E-02	1.4E-04	0.92313	NA	NA	NA
SDE (Fathy et al., 2020a)	−1.1924	3.199E-03	3.799E-05	−1.87E-04	22.817	2.903E-02	1.202E-04	1.0526	NA	NA	NA
ALO (Ali et al., 2017)	−0.9438	3.4734E-03	9.7898E-05	−1.1811E-04	24.0000	1.36E-02	1.6530E-04	1.1513	1.3352	1.4481	0.0982
TLBO-DE (Turgut and Coban, 2016)	−0.8532	2.6505E-03	8.0016E-05	−1.3601E-04	15.6514	3.64E-02	1.00E-04	7.2776677	7.2776677	7.2776677	7.542E-15
STLBO (Niu et al., 2014)	−0.8532	2.5843E-03	7.6892E-05	−1.1541E-04	12.6079	3.29E-02	1.00E-04	7.6266	NA	NA	NA
ISSA (Sultan et al., 2020)	−0.8616	3.1548E-03	9.7857E-05	−1.5423E-04	22.8812	5.47E-02	1.0016E-04	0.6434	0.8698	1.8744	19.96834
CEPSO (Özdemir, 2021)	−0.8555	2.4023E-03	5.7420E-05	−1.5838E-04	24.9999	5.54E-02	1.0000E-04	0.6112	NA	NA	NA
JAYA-NM (Gong and Cai, 2013)	−1.19966	3.55E-03	6.00E-05	−1.200E-04	13.2287	3.334E-02	1.1026E-04	5.2513	NA	NA	NA
MFFA (Menesy et al., 2021)	−1.00183	2.61199E-03	3.99591E-05	−1.55872E-04	23	5.455E-02	1.0000E-04	0.64202	0.72676	1.08608	9.96261
QPFA	−0.9934	4.60E-03	8.81E-05	−1.30E-04	12.9868	6.17E-02	1.00E-04	0.5934830	0.6102414	**0.6103414**	**7.00E-4**

**Bold numbers represent the best results.*

after optimization with the published literature in recent years, QPFA get a better result than these powerful optimizers.

7 CONCLUSION AND FUTURE WORK

In this paper, a new quantum coding pathfinder optimization algorithm is proposed, which uses probability angles to represent individuals and probability magnitudes to represent the probabilities of 1 and 0 in quantum computing, and maps them to the solution space of the optimization problem through mapping relations. The characteristics of quantum computing make one individual in QPFA correspond to two individuals in the solution space, which increases the population diversity and improves the exploration ability of PFA. Quantum revolving gate and pathfinder update strategies are used for iterative updates of probability angles, and quantum non-gates help QPFA to jump out of local optimal solutions. QPFA is applied to the determination of PEMFC location parameters, and three commercial types of PEMFC are studied. QPFA achieves the best results for all three PEMFC model parameter extraction, and the Friedman test also shows that the performance of QPFA ranks the first among all algorithms. The results obtained from QPFA search optimization were compared with those from published literature, and the results obtained by QPFA have higher stability and accuracy values. Various implementations of the group pathfinder algorithm will be considered in the future and applied to more types of PEMFC parameter extraction problems.

DATA AVAILABILITY STATEMENT

The raw data supporting the conclusion of this article will be made available by the authors, without undue reservation.

AUTHOR CONTRIBUTIONS

NL: Investigation, experiment, writing—draft; GZ: experiment, formal analysis; YZ: supervision, writing—review and editing. WD: writing—review and editing. QL: supervision, writing—review and editing.

FUNDING

This work was supported by the National Science Foundation of China under Grant Nos. U21A20464, 62066005 and 61771087, and Program for Young Innovative Research Team in China University of Political Science and Law, under Grant No. 21CXTD02.

REFERENCES

Abdel-Basset, M., Mohamed, R., El-Fergany, A., Chakrabortty, R. K., and Ryan, M. J. (2021). Adaptive and efficient optimization model for optimal parameters of proton exchange membrane fuel cells: A comprehensive analysis. *Energy* 233, 121096. doi:10.1016/j.energy.2021.121096

Abdel-Basset, M., Mohamed, R., Elhoseny, M., Chakrabortty, R. K., and Ryan, M. J. (2021). An efficient heap-based optimization algorithm for parameters identification of proton exchange membrane fuel cells model: Analysis and case studies. *Int. J. Hydrogen Energy* 46 (21), 11908–11925. doi:10.1016/j.ijhydene.2021.01.076

Ali, M., El-Hameed, M., and Farahat, M. (2017). Effective parameters' identification for polymer electrolyte membrane fuel cell models using grey wolf optimizer. *Renew. Energy* 111, 455–462. doi:10.1016/j.renene.2017.04.036

Amphlett, J. C., Baumert, R. M., Mann, R. F., Peppley, B. A., Roberge, P. R., and Harris, T. J. (1995). Performance modeling of the ballard mark IV solid polymer electrolyte fuel cell: I. Mechanistic model development. *J. Electrochem. Soc.* 142 (1), 1–8. doi:10.1149/1.2043866

Ashraf, H., Abdellatif, S. O., Elkholy, M. M., and El-Fergany, A. A. (2022). Computational techniques based on artificial intelligence for extracting optimal parameters of PEMFCs: Survey and insights. *Arch. Comput. Methods Eng.* 2022, 1–30. doi:10.1007/s11831-022-09721-y

Ben Messaoud, R. (2021). Parameters determination of proton exchange membrane fuel cell stack electrical model by employing the hybrid water cycle moth-flame optimization algorithm. *Int. J. Energy Res.* 45 (3), 4694–4708. doi:10.1002/er.6065

Benioff, P. (1982). Quantum mechanical Hamiltonian models of Turing machines. *J. Stat. Phys.* 29 (3), 515–546. doi:10.1007/bf01342185

Busquet, S., Hubert, C.-E., Labbé, J., Mayer, D., and Metkemeijer, R. (2004). A new approach to empirical electrical modelling of a fuel cell, an electrolyser or a regenerative fuel cell. *J. Power sources* 134 (1), 41–48. doi:10.1016/j.jpowsour.2004.02.018

Cao, Y., Li, Y., Zhang, G., Jermsittiparsert, K., and Razmjooy, N. (2019). Experimental modeling of PEM fuel cells using a new improved seagull optimization algorithm. *Energy Rep.* 5, 1616–1625. doi:10.1016/j.egyr.2019.11.013

Chen, Y., and Wang, N. (2019). Cuckoo search algorithm with explosion operator for modeling proton exchange membrane fuel cells. *Int. J. Hydrogen Energy* 44 (5), 3075–3087. doi:10.1016/j.ijhydene.2018.11.140

Chuahy, F. D., and Kokjohn, S. L. (2019). Solid oxide fuel cell and advanced combustion engine combined cycle: A pathway to 70% electrical efficiency. *Appl. Energy* 235, 391–408. doi:10.1016/j.apenergy.2018.10.132

Dey, S., Bhattacharyya, S., and Maulik, U. (2014). Quantum inspired genetic algorithm and particle swarm optimization using chaotic map model based interference for gray level image thresholding. *Swarm Evol. Comput.* 15, 38–57. doi:10.1016/j.swevo.2013.11.002

Diab, A. A. Z., Ali, H., Abdul-Ghaffar, H., Abdelsalam, H. A., and Sattar, M. A. E. (2021). Accurate parameters extraction of PEMFC model based on metaheuristics algorithms. *Energy Rep.* 7, 6854–6867. doi:10.1016/j.egyr.2021.09.145

Diab, A. A. Z., Tolba, M. A., El-Magd, A. G. A., Zaky, M. M., and El-Rifaie, A. M. (2020). Fuel cell parameters estimation via marine predators and political optimizers. *IEEE Access* 8, 166998–167018. doi:10.1109/access.2020.3021754

El-Fergany, A. A. (2018). Electrical characterisation of proton exchange membrane fuel cells stack using grasshopper optimiser. *IET Renew. Power Gener.* 12 (1), 9–17. doi:10.1049/iet-rpg.2017.0232

El-Fergany, A. A. (2018). Extracting optimal parameters of PEM fuel cells using Salp Swarm Optimizer. *Renew. Energy* 119, 641–648. doi:10.1016/j.renene.2017.12.051

Elsayed, S. K., Agwa, A. M., Elattar, E. E., and El-Fergany, A. (2021). Steady-state modelling of PEM fuel cells using gradient-based optimizer. *Dyna (Medellin).* 96 (5), 520–527. doi:10.6036/10099

Fathy, A., Abd Elaziz, M., and Alharbi, A. G. (2020). A novel approach based on hybrid vortex search algorithm and differential evolution for identifying the optimal parameters of PEM fuel cell. *Renew. Energy* 146, 1833–1845. doi:10.1016/j.renene.2019.08.046

Fathy, A., Abdel Aleem, S. H., and Rezk, H. (2021). A novel approach for PEM fuel cell parameter estimation using LSHADE-EpSin optimization algorithm. *Int. J. Energy Res.* 45 (5), 6922–6942. doi:10.1002/er.6282

Fathy, A., and Rezk, H. (2018). Multi-verse optimizer for identifying the optimal parameters of PEMFC model. *Energy* 143, 634–644. doi:10.1016/j.energy.2017.11.014

Fathy, A., Rezk, H., and Ramadan, H. S. M. (2020). Recent moth-flame optimizer for enhanced solid oxide fuel cell output power via optimal parameters extraction process. *Energy* 207, 118326. doi:10.1016/j.energy.2020.118326

Gong, W., and Cai, Z. (2013). Accelerating parameter identification of proton exchange membrane fuel cell model with ranking-based differential evolution. *Energy* 59, 356–364. doi:10.1016/j.energy.2013.07.005

Gouda, E. A., Kotb, M. F., and El-Fergany, A. A. (2021). Investigating dynamic performances of fuel cells using pathfinder algorithm. *Energy Convers. Manag.* 237, 114099. doi:10.1016/j.enconman.2021.114099

Gouda, E. A., Kotb, M. F., and El-Fergany, A. A. (2021). Jellyfish search algorithm for extracting unknown parameters of PEM fuel cell models: Steady-state performance and analysis. *Energy* 221, 119836. doi:10.1016/j.energy.2021.119836

Grover, L. K. (2001). From Schrödinger's equation to the quantum search algorithm. *Pramana -. J. Phys.* 56 (2), 333–348. doi:10.1007/s12043-001-0128-3

Guo, X., Zhang, H., Hu, Z., Hou, S., Ni, M., and Liao, T. (2021). Energetic, exergetic and ecological evaluations of a hybrid system based on a phosphoric acid fuel cell and an organic Rankine cycle. *Energy* 217, 119365. doi:10.1016/j.energy.2020.119365

Gupta, J., Nijhawan, P., and Ganguli, S. (2021). Optimal parameter estimation of PEM fuel cell using slime mould algorithm. *Int. J. Energy Res.* 45 (10), 14732–14744. doi:10.1002/er.6750

Hachana, O., and El-Fergany, A. A. (2022). Efficient PEM fuel cells parameters identification using hybrid artificial bee colony differential evolution optimizer. *Energy* 250, 123830. doi:10.1016/j.energy.2022.123830

Hasanien, H. M., Shaheen, M. A., Turky, R. A., Qais, M. H., Alghuwainem, S., Kamel, S., et al. (2022). Precise modeling of PEM fuel cell using a novel Enhanced Transient Search Optimization algorithm. *Energy* 247, 123530. doi:10.1016/j.energy.2022.123530

Ido, A., and Kawase, M. (2020). Development of a tubular molten carbonate direct carbon fuel cell and basic cell performance. *J. Power sources* 449, 227483. doi:10.1016/j.jpowsour.2019.227483

Inci, M., and Türksoy, Ö. (2019). Review of fuel cells to grid interface: Configurations, technical challenges and trends. *J. Clean. Prod.* 213, 1353–1370. doi:10.1016/j.jclepro.2018.12.281

Kandidayeni, M., Macias, A., Khalatbarisoltani, A., Boulon, L., and Kelouwani, S. (2019). Benchmark of proton exchange membrane fuel cell parameters extraction with metaheuristic optimization algorithms. *Energy* 183, 912–925. doi:10.1016/j.energy.2019.06.152

Kennedy, J., and Eberhart, R. (1995). "Particle swarm optimization," in Proceedings of ICNN'95-international conference on neural networks (Perth, WA, Australia: IEEE), 1942–1948.

Li, J., Gao, X., Cui, Y., Hu, J., Xu, G., and Zhang, Z. (2020). Accurate, efficient and reliable parameter extraction of PEM fuel cells using shuffled multi-simplexes search algorithm. *Energy Convers. Manag.* 206, 112501. doi:10.1016/j.enconman.2020.112501

Li, S., Chen, H., Wang, M., Heidari, A. A., and Mirjalili, S. (2020). Slime mould algorithm: A new method for stochastic optimization. *Future Gener. Comput. Syst.* 111, 300–323. doi:10.1016/j.future.2020.03.055

Mann, R. F., Amphlett, J. C., Hooper, M. A., Jensen, H. M., Peppley, B. A., and Roberge, P. R. (2000). Development and application of a generalised steady-state electrochemical model for a PEM fuel cell. *J. Power sources* 86 (1-2), 173–180. doi:10.1016/s0378-7753(99)00484-x

Menesy, A. S., Sultan, H. M., Korashy, A., Kamel, S., and Jurado, F. (2021). A modified farmland fertility optimizer for parameters estimation of fuel cell models. *Neural comput. Appl.* 33 (18), 12169–12190. doi:10.1007/s00521-021-05821-1

Miao, D., Chen, W., Zhao, W., and Demsas, T. (2020). Parameter estimation of PEM fuel cells employing the hybrid grey wolf optimization method. *Energy* 193, 116616. doi:10.1016/j.energy.2019.116616

Mirjalili, S., and Lewis, A. (2016). The whale optimization algorithm. *Adv. Eng. Softw.* 95, 51–67. doi:10.1016/j.advengsoft.2016.01.008

Mirjalili, S., Mirjalili, S. M., and Lewis, A. (2014). Grey wolf optimizer. *Adv. Eng. Softw.* 69, 46–61. doi:10.1016/j.advengsoft.2013.12.007

Mirjalili, S. (2016). Sca: A sine cosine algorithm for solving optimization problems. *Knowledge-based Syst.* 96, 120–133. doi:10.1016/j.knosys.2015.12.022

Mossa, M. A., Kamel, O. M., Sultan, H. M., and Diab, A. A. Z. (2021). Parameter estimation of PEMFC model based on Harris Hawks' optimization and atom search optimization algorithms. *Neural comput. Appl.* 33 (11), 5555–5570. doi:10.1007/s00521-020-05333-4

Niu, Q., Zhang, H., and Li, K. (2014). An improved TLBO with elite strategy for parameters identification of PEM fuel cell and solar cell models. *Int. J. Hydrogen Energy* 39 (8), 3837–3854. doi:10.1016/j.ijhydene.2013.12.110

Özdemir, M. T. (2021). Optimal parameter estimation of polymer electrolyte membrane fuel cells model with chaos embedded particle swarm optimization. *Int. J. Hydrogen Energy* 46 (30), 16465–16480. doi:10.1016/j.ijhydene.2020.12.203

Pourrahmani, H., Siavashi, M., and Moghimi, M. (2019). Design optimization and thermal management of the PEMFC using artificial neural networks. *Energy* 182, 443–459. doi:10.1016/j.energy.2019.06.019

Priya, K., Babu, T. S., Balasubramanian, K., Sathish Kumar, K., and Rajasekar, N. (2015). A novel approach for fuel cell parameter estimation using simple genetic algorithm. *Sustain. Energy Technol. Assessments* 12, 46–52. doi:10.1016/j.seta.2015.09.001

Priya, K., and Rajasekar, N. (2019). Application of flower pollination algorithm for enhanced proton exchange membrane fuel cell modelling. *Int. J. Hydrogen Energy* 44 (33), 18438–18449. doi:10.1016/j.ijhydene.2019.05.022

Priya, K., Sathishkumar, K., and Rajasekar, N. (2018). A comprehensive review on parameter estimation techniques for Proton Exchange Membrane fuel cell modelling. *Renew. Sustain. Energy Rev.* 93, 121–144.

Qin, F., Liu, P., Niu, H., Song, H., and Yousefi, N. (2020). Parameter estimation of PEMFC based on improved fluid search optimization algorithm. *Energy Rep.* 6, 1224–1232. doi:10.1016/j.egyr.2020.05.006

Rao, R. (2016). Jaya: A simple and new optimization algorithm for solving constrained and unconstrained optimization problems. *Int. J. Industrial Eng. Comput.* 7 (1), 19–34.

Rao, Y., Shao, Z., Ahangarnejad, A. H., Gholamalizadeh, E., and Sobhani, B. (2019). Shark Smell Optimizer applied to identify the optimal parameters of the proton exchange membrane fuel cell model. *Energy Convers. Manag.* 182, 1–8. doi:10.1016/j.enconman.2018.12.057

Rezk, H., Ferahtia, S., Djeroui, A., Chouder, A., Houari, A., Machmoum, M., et al. (2022). Optimal parameter estimation strategy of PEM fuel cell using gradient-based optimizer. *Energy* 239, 122096.

Rizk-Allah, R. M., and El-Fergany, A. A. (2021). Artificial ecosystem optimizer for parameters identification of proton exchange membrane fuel cells model. *Int. J. Hydrogen Energy* 46 (75), 37612–37627. doi:10.1016/j.ijhydene.2020.06.256

Saebea, D., Chaiburi, C., and Authayanun, S. (2019). Model based evaluation of alkaline anion exchange membrane fuel cells with water management. *Chem. Eng. J.* 374, 721–729. doi:10.1016/j.cej.2019.05.200

Salim, R., Nabag, M., Noura, H., and Fardoun, A. (2015). The parameter identification of the Nexa 1.2 kW PEMFC's model using particle swarm optimization. *Renew. Energy* 82, 26–34. doi:10.1016/j.renene.2014.10.012

Sayed, E. T., Abdelkareem, M. A., Alawadhi, H., Elsaid, K., Wilberforce, T., and Olabi, A. (2021). Graphitic carbon nitride/carbon brush composite as a novel anode for yeast-based microbial fuel cells. *Energy* 221, 119849. doi:10.1016/j.energy.2021.119849

Seleem, S. I., Hasanien, H. M., and El-Fergany, A. A. (2021). Equilibrium optimizer for parameter extraction of a fuel cell dynamic model. *Renew. Energy* 169, 117–128. doi:10.1016/j.renene.2020.12.131

Selem, S. I., Hasanien, H. M., and El-Fergany, A. A. (2020). Parameters extraction of PEMFC's model using manta rays foraging optimizer. *Int. J. Energy Res.* 44 (6), 4629–4640. doi:10.1002/er.5244

Shaheen, M. A., Hasanien, H. M., El Moursi, M., and El-Fergany, A. A. (2021). Precise modeling of PEM fuel cell using improved chaotic MayFly optimization algorithm. *Int. J. Energy Res.* 45 (13), 18754–18769. doi:10.1002/er.6987

Shiyong, L. (2007). Quantum particle swarms algorithm for continuous space optimization. *Chin. J. Quantum Electron.* 24 (5), 569.

Sultan, H. M., Menesy, A. S., Kamel, S., Selim, A., and Jurado, F. (2020). Parameter identification of proton exchange membrane fuel cells using an improved salp swarm algorithm. *Energy Convers. Manag.* 224, 113341. doi:10.1016/j.enconman.2020.113341

Turgut, O. E., and Coban, M. T. (2016). Optimal proton exchange membrane fuel cell modelling based on hybrid Teaching Learning Based Optimization–Differential Evolution algorithm. *Ain Shams Eng. J.* 7 (1), 347–360. doi:10.1016/j.asej.2015.05.003

Wolpert, D. H., and Macready, W. G. (1997). No free lunch theorems for optimization. *IEEE Trans. Evol. Comput.* 1 (1), 67–82. doi:10.1109/4235.585893

Xu, S., Wang, Y., and Wang, Z. (2019). Parameter estimation of proton exchange membrane fuel cells using eagle strategy based on JAYA algorithm and Nelder-Mead simplex method. *Energy* 173, 457–467. doi:10.1016/j.energy.2019.02.106

Yang, Z., Liu, Q., Zhang, L., Dai, J., and Razmjooy, N. (2020). Model parameter estimation of the PEMFCs using improved barnacles mating optimization algorithm. *Energy* 212, 118738. doi:10.1016/j.energy.2020.118738

Yapici, H., and Cetinkaya, N. (2019). A new meta-heuristic optimizer: Pathfinder algorithm. *Appl. soft Comput.* 78, 545–568. doi:10.1016/j.asoc.2019.03.012

Yousri, D., Mirjalili, S., Machado, J. T., Thanikanti, S. B., elbaksawi, O., and Fathy, A. (2021). Efficient fractional-order modified Harris Hawks optimizer for proton exchange membrane fuel cell modeling. *Eng. Appl. Artif. Intell.* 100, 104193. doi:10.1016/j.engappai.2021.104193

Zhang, L., and Wang, N. (2018). Application of coRNA-GA based RBF-NN to model proton exchange membrane fuel cells. *Int. J. Hydrogen Energy* 43 (1), 329–340. doi:10.1016/j.ijhydene.2017.11.027

Conflict of Interest: The authors declare that the research was conducted in the absence of any commercial or financial relationships that could be construed as a potential conflict of interest.

Publisher's Note: All claims expressed in this article are solely those of the authors and do not necessarily represent those of their affiliated organizations, or those of the publisher, the editors and the reviewers. Any product that may be evaluated in this article, or claim that may be made by its manufacturer, is not guaranteed or endorsed by the publisher.